ASSESSING LOCAL SNOW VARIABILITY USING A NETWORK OF ULTRASONIC SNOW DEPTH SENSORS

by

Erik Thorsten Boe

A thesis

submitted in partial fulfillment

of the requirements for the degree of

Master of Science in Hydrologic Sciences

Boise State University

December 2013

BOISE STATE UNIVERSITY GRADUATE COLLEGE

DEFENSE COMMITTEE AND FINAL READING APPROVALS

of the thesis submitted by

Erik Thorsten Boe

Thesis Title: Assessing Local Snow Variability Using a Network of Ultrasonic Snow Depth Sensors

Date of Final Oral Examination: 04 October 2013

The following individuals read and discussed the thesis submitted by student Erik Thorsten Boe, and they evaluated his presentation and response to questions during the final oral examination. They found that the student passed the final oral examination.

James P. McNamara, Ph.D.	Chair, Supervisory Committee
Hans-Peter Marshall, Ph.D.	Member, Supervisory Committee
Alejandro N. Flores, Ph.D.	Member, Supervisory Committee

The final reading approval of the thesis was granted by James McNamara, Ph.D., Chair of the Supervisory Committee. The thesis was approved for the Graduate College by John R. Pelton, Ph.D., Dean of the Graduate College.

ACKNOWLEDGEMENTS

I would like to thank my advisor, committee, Boise State University staff and students, coworkers, and family for their support during this process. Many thanks to my advisor, Dr. James P. McNamara, for his countless hours of time, encouragement, and well recognized expertise throughout the duration of this investigation. Thanks to my committee, Dr. Hans-Peter Marshall and Dr. Alejandro N. Flores, who were always willing to help and provide a wide breadth of knowledge and advice that was invaluable. Thanks to Pam Aishlin, Patrick Kormos, Dave Eiriksson, Alison Burnop, Brian Anderson, Alden Shallcross, and others; they were an incredible research group to work with, always willing to lend a hand with technical challenges in the office or spend countless hours in the field. A special thanks to all my amazing kids, sister and brother-in-law, extended family, and friends; they have no idea how much I am thankful for all their support. And finally, I would like to thank my wife Tiara who is the most patient, encouraging, and helpful person I have ever known; I am forever grateful.

Funding for this research was provided by the National Weather Service and National Oceanic and Atmospheric Administration. Funding for my tuition, fees, and books was provided by the Trade Adjustment Assistance program and the Workforce Investment Act.

ABSTRACT

During the 2009-2010 winter season, 21 inexpensive ultrasonic snow depth (USD) sensors were constructed and installed, in addition to two standard Judd USD sensors, at Treeline and Lower Deer Point sites located within the snow dominated Dry Creek Experimental Watershed, near Boise, Idaho. Six USD sensors, including a single Judd Communications USD sensor, were installed at the Treeline site along a northeast to southwest transect of the small 0.02 km^2 catchment. Seventeen USD sensors, including a single Judd Communications USD sensor, were installed at Lower Deer Point in a randomized stratified pattern with respect to aspect and vegetation to reflect the nature of the ridge knob site. The purpose of this study was to investigate the local variability of SWE in the form of new fallen snow and assess how well data obtained from standard precipitation gauges represent local conditions. Spatial distributions of new snow depth were converted to estimated new SWE, based off of the relationship between USD measurements of new fallen snow depth and new fallen snow density estimates collected from storm boards placed in a stratified pattern with respect to USD site locations at Treeline and Lower Deer Point. In all, on a storm by storm basis, Lower Deer Point and Treeline precipitation gauges were found to underestimate water accumulation by approximately 16% to 30% and 18% to 26%, respectively. These findings are consistent with what is typically observed from uncorrected weighing-type precipitation gauge measurements. Additionally, variability associated with new fallen SWE estimates was

found to increase with increasing snow accumulation totals, which was consistent with previous field studies.

TABLE OF CONTENTS

LIST OF TABLES

LIST OF FIGURES

CHAPTER 1: INTRODUCTION

Water stored as snow provides approximately 80 percent of streamflow and the vast majority of fresh water for domestic and irrigation purposes in the Western United states (Pagano and Garen, 2005). Add to this the well documented occurrences of increased climate variability and population growth, we find that significantly more pressure is being placed on hydrologic modeling as the basis for decisions regarding water resource policy, management, regulation, and program evaluation (Larson and Peck, 1974; Haan et al., 1995; Kunkel et al., 2007; Harmel and Smith, 2007). A greater understanding of uncertainties associated with streamflow forecasts is essential for operational hydrologic models (Larson and Peck, 1974; Goodison, 1978; Peck, 1997; Yang et al., 2000; Slater and Clark, 2006; Harmel and Smith, 2007).

In snow dominated catchments, streamflow forecast models must account for the spatial and temporal nature of snow water input into the system (Peck, 1997; Clark and Slater, 2006; Slater and Clark, 2006; Elder et al., 2009). This is accomplished by incorporating snowmelt models, such as SNOW-17 (Anderson, 1973) and the Snowmelt-Runoff Model (Martinec et al., 2008; Burnop, 2012), that route snowmelt water into the system based on local precipitation and temperature observations obtained from measurement equipment (Anderson, 1973; Slater and Clark, 2006; Mertinec et al., 2008). Uncertainty inherent to these hydrologic models can be classified into three general categories; model uncertainty, forcing uncertainty, and uncertainty inherent in natural

processes (Vicens et al., 1975; Slater and Clark, 2006; Harmel and Smith, 2007). Of these sources of uncertainty, measurement (forcing) uncertainty is commonly regarded as an important factor influencing model performance but is rarely quantified (Larson and Peck, 1974; Peck, 1997; Yang et al., 2000; Slater and Clark, 2006; Harmel and Smith 2007). In particular, precipitation measurements used as model forcings are considered by many as the most important factor to successful hydrologic models (Larson and Peck, 1974; Peck, 1997; Yang et al., 2000). The accuracy of streamflow forecasts in snow dominated catchments is primarily influenced by the accuracy of the snow accumulation and resulting snow water equivalent (SWE) estimates (Slater and Clark, 2006; Elder et al., 2009). Herein lies the challenge, snow precipitation observations are obtained from gauges with high gauge catch deficiencies (Larson and Peck, 1974; Yang et al., 2000; Dingman, 2008), which introduce significant and unknown uncertainties into snowmelt models (Harmel and Smith, 2007).

A significant amount of work has been directed toward ascertaining measurement uncertainty associated with snow precipitation gauge observations. Larson and Peck (1974) found that gauge catch deficiencies for snow precipitation measurement using weighing-type bucket gauges varied greatly with respect to wind speed. During the study, Alter shielded weighing-type bucket gauges experienced gauge catch deficiencies of 28% at 10 mph and 45% at 20 mph while unshielded gauges experienced gauge catch deficiencies of 45% at 10 mph and 70% at 20 mph (Larson and Peck, 1974). Since that time, there have been a number of schemes to either reduce the gauge catch deficiencies associated with snow precipitation measurement or improve its estimation (Yang et al., 2000). While various wind shields such as the Alter, Canadian Nipher, and Wyoming

fence have reduced gauge catch deficiencies and continued tests have improved gauge catch deficiency estimates (Yang et al., 2000; Hansen and Davies, 2002; Fassnacht, 2004; Sevruk et al., 2009) the fact remains that significant errors are present and difficult to ascertain. An important note is that when considering these errors, especially as they relate to local conditions, one cannot overlook the impact of uncertainty associated with natural processes. The variable nature of natural controls such as wind, temperature, slope, aspect, and vegetation-type are contributing factors to precipitation measurement uncertainty as a whole. The act of quantifying measurement uncertainty of local conditions inherently captures uncertainty associated with influential natural processes. All of which begs the question of how representative snow precipitation gauge measurements are of local conditions. To answer this question, one must look at alternative approaches of snow precipitation measurement. One such method involves the use of ultrasonic snow depth (USD) sensors (Goodison et al., 1984; Goodison et al., 1988; Ryan et al., 2008a,b).

USD sensors have been in use since the 1980s when Goodison et al. (1984) successfully tested them at remote Canadian locations. More recently, a USD sensor has been standard issue and proven effective for Snow Telemetry (SNOTEL) sites located throughout the western United States. In 2005, Ryan et al. (2008a) evaluated the Judd Communications and Campbell Scientific SR-50 USD sensors. Both USD sensors produced promising results, but that they tended to underestimate actual accumulation to a certain degree. The study attributed the underestimate of snow accumulation to site selection as well as the need for multiple or clusters of USD sensors for a given location. In 2006, Ryan et al. (2008b) initiated the National Weather Service (NWS) Automated

Surface Observation System (ASOS) network in an effort to replace human observers with automated sensors for monitoring snow accumulation. As part of this program, 3 USD sensors were placed at each of 17 NWS monitoring locations over the course of the 2006-2007 winter season. Important conclusions include: (1) incorporating multiple USD sensors improved the overall accuracy of site snow accumulation measurements and (2) even at sites with exposure to significant winds, the network of 3 USD sensors provided relatively accurate and representative snow accumulation totals for the station (Ryan et al., 2008b). Overall, findings by Goodison et al. (1984) and Ryan et al. (2008b) suggest that networks composed of multiple USD sensors have the ability to effectively describe snow accumulation and variability at a local scale with one caveat, the price. USD sensors can be quite expensive (~$900 without logger) especially when considering large networks composed of multiple sensors. Obtaining a spatially significant number of snow accumulation observations using USD sensors that are low cost solicits a novel approach. The goal of this study is to: (1) develop inexpensive USD sensors that have comparable performance characteristics to commercially available alternatives, (2) use USD sensor networks to investigate the local variability of SWE in the form of new fallen snow, (3) and develop uncertainty estimates to assess how well data obtained from standard precipitation gauges represents local conditions.

CHAPTER 2: SITE DESCRIPTION

The study was conducted at Treeline and Lower Deer Point sites situated within the greater Dry Creek Experimental Watershed (DCEW, 27 km^2) located to the north of Boise, Idaho.

The Treeline site is located in a vegetation transition zone at the edge of a sagebrush steppe ecotone just below the mixed conifer forested regions of the DCEW (Williams et al., 2009; Anderson, 2011; Eiriksson, 2012). Historically, Treeline receives a mix of rain or snow throughout the winter season with relative weightings varying from year to year. Treeline encompasses 0.02 km^2 and is located at an elevation of 1620 m (Williams et al., 2009). The catchment trends from northwest to southeast with steep opposing northeast and southwest slope aspects. Treeline is outfitted with standard meteorological instrumentation that includes two weighing bucket precipitation gauges, one of which is equipped with an Alter shield, and a Judd Communications ultrasonic snow depth sensor (Figure 1). The two precipitation gauges and ultrasonic snow depth sensor are located on the northeast slope. Historically, Treeline is located within a rain-snow transition elevation zone.

The Lower Deer Point site is located on a ridge knob surrounded by a mixed conifer forest at an elevation of 1850 m with slope aspect exposures ranging from east to west (Anderson, 2011), clockwise (Figure 2). Locally, Lower Deer Point site contains a mix of shrubs including alder and dense distributions of ceanothus across all aspects with

the mixed conifer forest located from northern to eastern aspects (Figure 2). Lower Deer Point is outfitted with standard meteorological instrumentation that includes two alter shielded weighing bucket precipitation gauges and a Judd Communications ultrasonic snow depth sensor. The ultrasonic snow depth sensor and one of the precipitation gauges are located on the ridge, while the other precipitation gauge is located on the eastern slope just above the forested area (Figure 2).

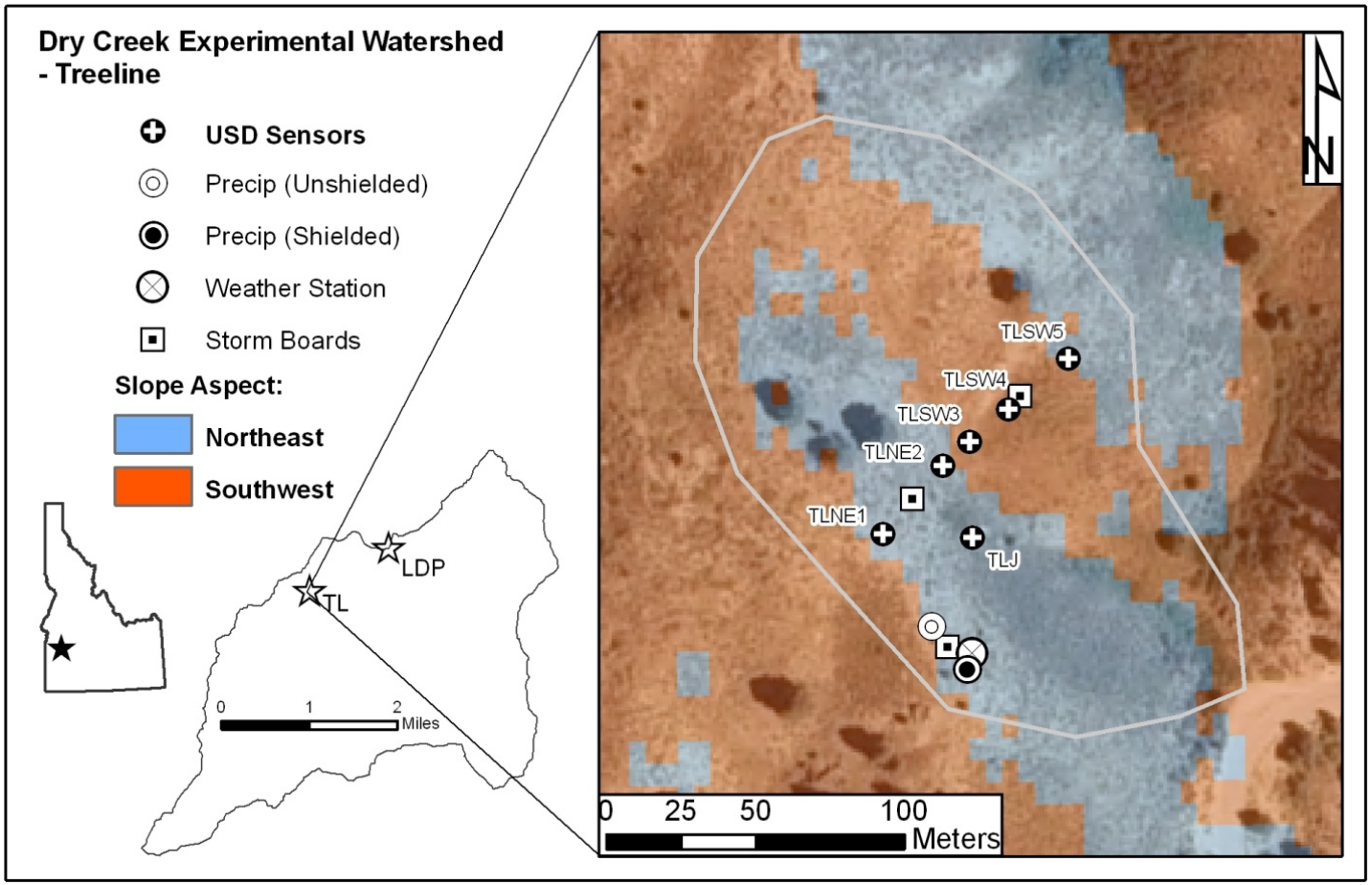

Figure 1 Treeline site map with aspect classification

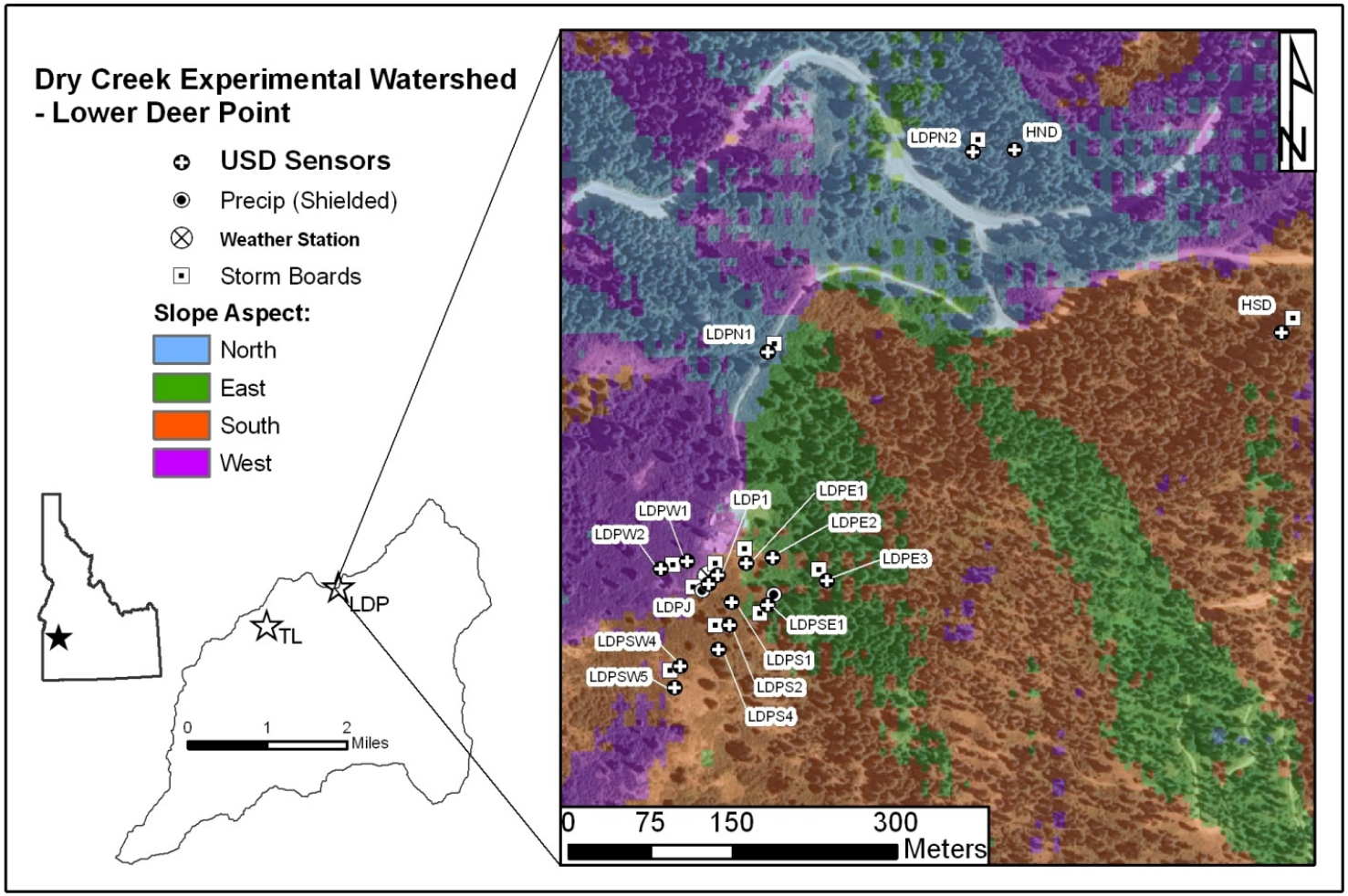

Figure 2 Lower Deer Point site map with aspect classification

CHAPTER 3: METHODS

3.1 Study Design - Snow Depth Measurements

Ultrasonic snow depth instruments have been widely used to measure snow accumulation in recent years having been under development since the early 1980s (Goodison et al., 1984; Ryan et al., 2008a,b). However, large networks of ultrasonic sensors have not been implemented due to large upfront costs associated with equipment purchases. Obtaining a spatially and statistically significant number snow accumulation observations using ultrasonic sensors that are low cost along with performance characteristics comparable to commercially available alternatives solicits a novel approach for this investigation. The following inexpensive snow depth sensors were designed, constructed, and tested to meet both the scope and budget of the study.

3.1.1 Theory of Design

Ultrasonic snow depth sensors operate by emitting an ultrasonic pulse (40 kHz to 50 kHz) and measuring the time it takes for the sound pulse to reflect off the surface of the snow and return to the transceiver (Goodison et al., 1984, Ryan et al.; 2008a,b). Since the velocity of sound waves vary as a function air temperature, ultrasonic velocity must be compensated with Equation (1) obtained from Ryan et al. (2008a,b).

$$V_{sound} = 331.4\left(\frac{T_a}{273.15}\right)^{\frac{1}{2}} \quad (1)$$

The ultrasonic pulse is projected downward in the shape of a cone, as illustrated in Figure 3, with incident angles between approximately 10 and 20 degrees depending on transceiver specifications. The base of the cone (Figure 3) must be clear of all objects (shrubs, hardware, etc) to prevent signal interference.

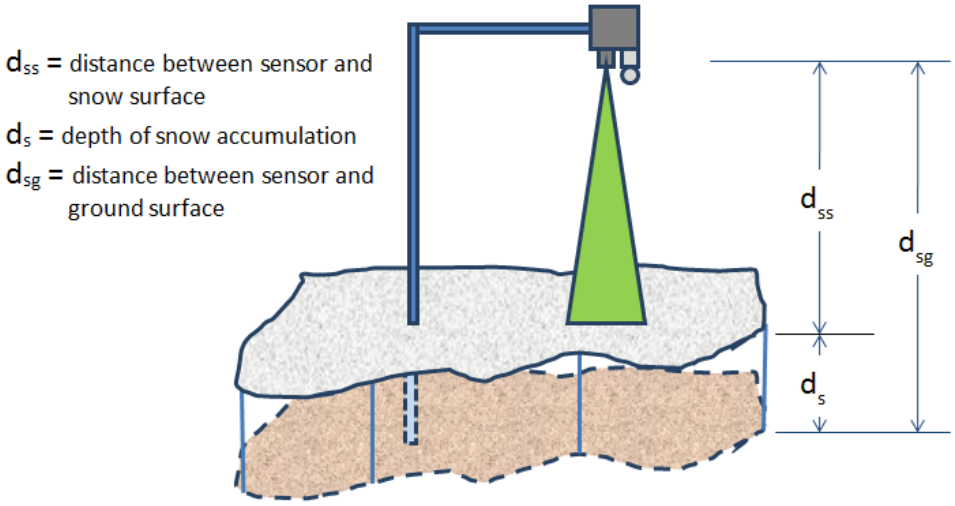

Figure 3 Ultrasonic snow depth sensor illustration

3.1.2 USD Design

The USD Design for this study was composed of an XL-MaxSonar EZ2 transceiver (Figure 4) to measure the distance between the sensor and the snow surface along with an onboard thermistor (Figure 5) to measure local air temperature conditions for compensation purposes. The complete list of components and potential suppliers are included in Table 1 and illustrated in Figure 4, Figure 5, and Figure 6. An important note is that fabrication of the USD sensors described in this study requires the ability to drill three holes and make three cuts prior to assembly. As illustrated in Figure 6, the XL-MaxSonar is held in place by a ½ inch PVC bushing affixed to the protective case.

The analog XL-MaxSonar EZ2 device requires three soldered pin connections for operation: (1) supply voltage of 5 volts, (2) connection to ground, and (3) analog output voltage. Over a 0 to 5 volt range, the analog output voltage signal is directly proportional to the distance between the transceiver and the surface by which the sound wave is reflected. MaxBotix, Inc. specifies a scaling factor of 0.0098 volts per inch (www.maxbotix.com). Manufacturer specifications for the XL-MaxSonar EZ2 are included in Appendix A. The thermistor package design involves a variable resister (thermistor) and reference resistor wired into a basic voltage divider circuit (Figure 5). Since air temperature is proportional to the resistance measured across the variable resistor, recorded voltage signals across the variable resistor can be used to determine air temperature. Similar to the transceiver, the thermistor and reference resistor package requires three soldered connections for operation: (1) supply voltage of 2.5 volts, (2) connection to ground, and (3) analog output voltage. Over a 0 to 2.5 volt range, the analog output voltage signal is directly analogous to air temperature using the relationship provided by the manufacturer, GE Measurement and Control Solutions (www.ge-mcs.com), in Appendix B.

The USD sensor itself was suspended above the ground and snow surface using ¾ inch rigid pipe all of which was strapped to a fence post that was hammered into the ground (Figure 7). The baseline power supply and data acquisition scheme is as follows. The standalone USD sensor power supply was composed of a 7 amp hour sealed lead acid battery and 5 volt regulator, which was capable of powering the USD sensor for approximately 30 days (Figure 7). Data acquisition was accomplished using a 4-channel U12 HOBO datalogger. All power supply and data acquisition components were placed

in a small insulated igloo container for protection from environmental conditions next to the base of the fence post (Figure 7).

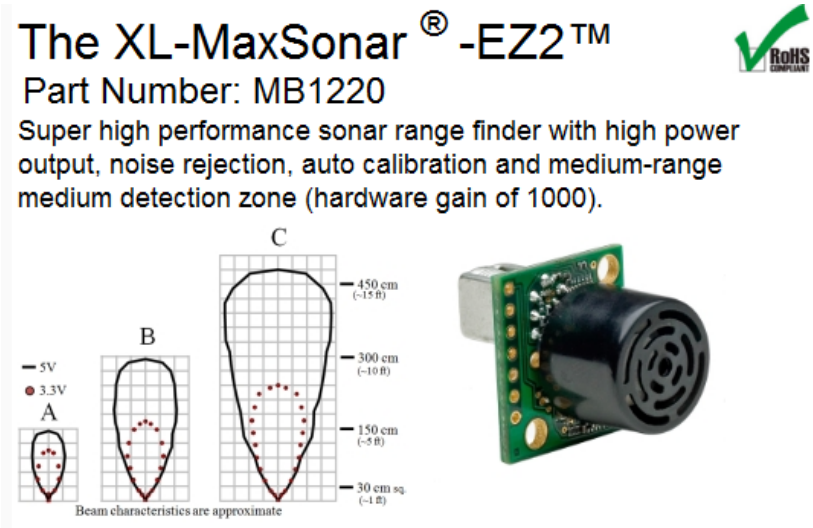

Figure 4 XL-MaxSonar EZ2 (www.maxbotix.com)

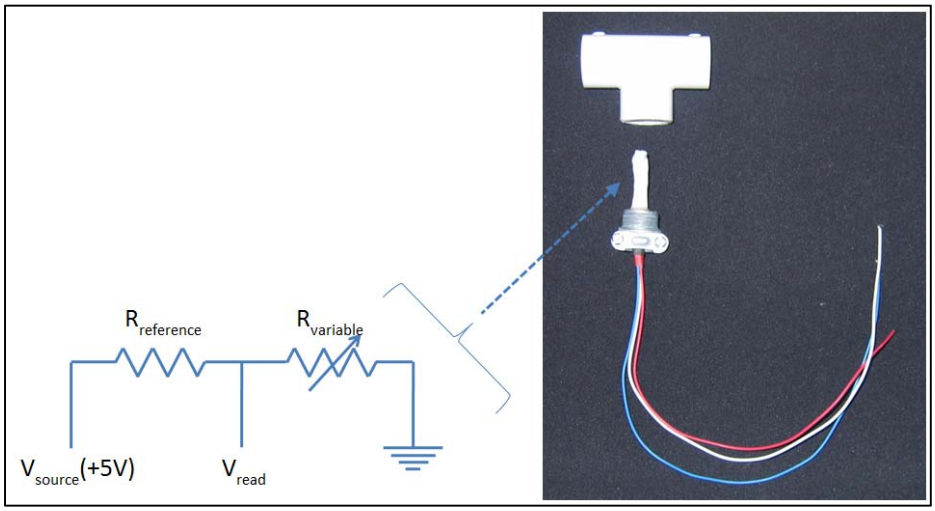

Figure 5 Thermistor design and construction

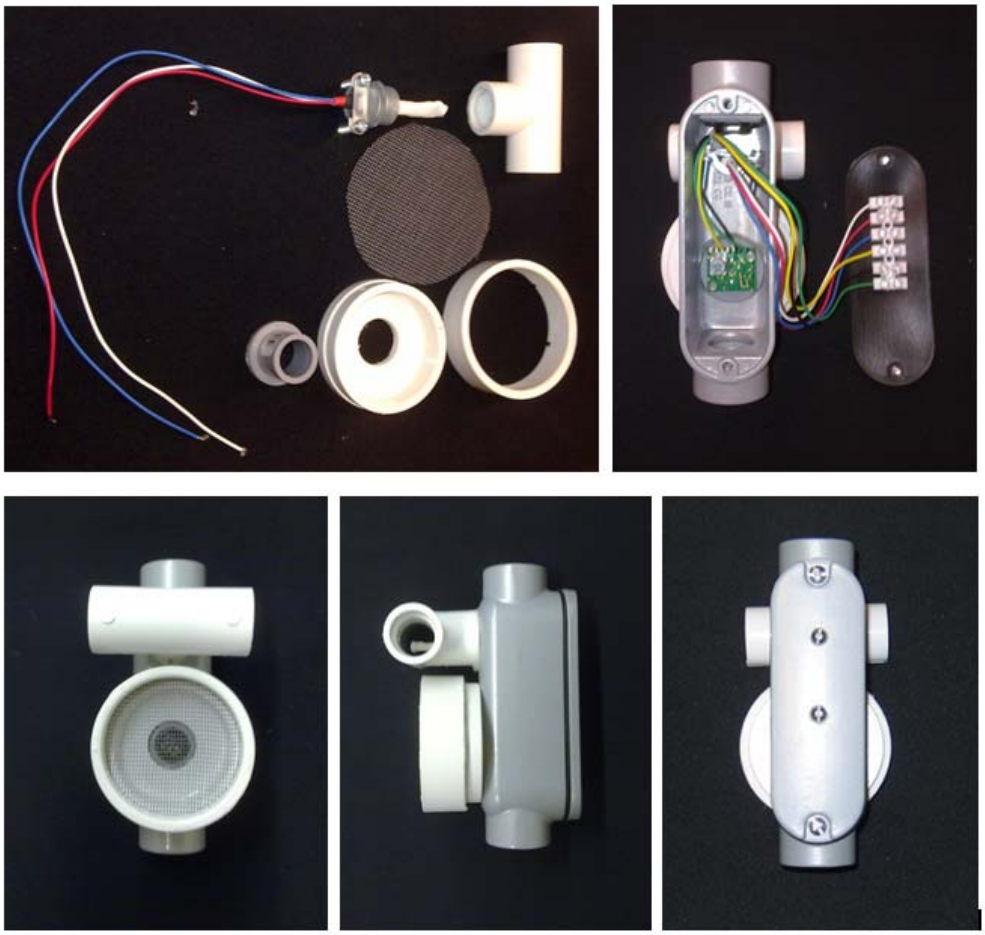

Figure 6 Ultrasonic snow depth sensor design

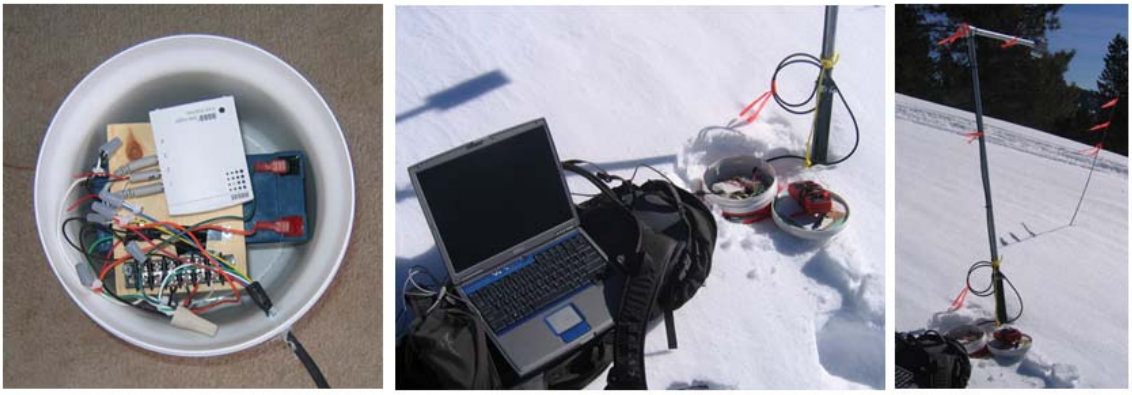

Figure 7 Power supply, data acquisition, and installation pictures

Table 1 Ultrasonic snow depth sensor parts list (2011)

Description	Product Name	Supplier	Price ($)
Sonar Sensor	XL-MaxSonar EZ2	www.maxbotix.com	39.95
Waterproof Case	3/4 in. Threaded Aluminum Conduit Body	www.homedepot.com	4.37
Sonar Compression Fitting	1/2 in. PVC Bushing	www.homedepot.com	0.60
Cover	2 in. PVC Plug	www.homedepot.com	1.88
Mesh Screen Cover	2 in PVC Coupling	www.homedepot.com	0.43
Mesh Screen Cover	2 in. Square Piece of Fiberglass Screen Material	www.homedepot.com	0.10
Epoxy	Epoxy	www.homedepot.com	1.00
Variable Resistor (Thermistor)	Thermistor NTC 10k Ohm 2% Toler	www.digikey.com	5.92
Resistor	Res 10k Ohm 1/4W 1% Metal Film	www.digikey.com	0.04
Heat-Shrink Tubing	PVC Heat-Shrink Tubing (1/8", 3/8")	www.mcmaster.com	1.00
Thermistor Connector	3/8 in. Twin-Screw Clamp Connector	www.homedepot.com	0.31
		Total =	**$55.60**

USD Accuracy and Uncertainty Estimate

To assess the accuracy and precision of the design, a random USD sensor was selected and placed above a level concrete slab, which represented a fixed target. The distance between the transceiver and the fixed target was measured with a steel tape measure and determined to be 120.0 cm. A total of 1440 USD sensor measurements were collected at 1 minute intervals over the course of a 24 hour period during which time air temperatures ranged from 0°C to 10°C. Since the distance between the USD sensor and the fixed target was constant, all 1440 measurements were lumped together to assess both the accuracy of the measurements and the degree to which they are influenced by air temperature. Two distributions of distance measurements are presented in Figure 8. The first distribution classified as “Raw” corresponds to raw measurements produced directly from the XL-MaxSonar EZ2 sensor, while the second distribution classified as

"Temp Comp" corresponds to distance measurements compensated for fluctuations in air temperature as described in Section 3.1.2. Results presented in Figure 8 suggest the following: (1) The USD sensors appear to effectively operate within the 1 cm resolution specification of commercially available alternatives such as the Judd Communications model. (2) With the interquartile range (75^{th} percent quartile minus the 25^{th} percent quartile) changing from 1.2 cm to 0.4 cm, air temperature compensation appeared to be both an effective and critical step to produce accurate snow accumulation measurements with higher precision.

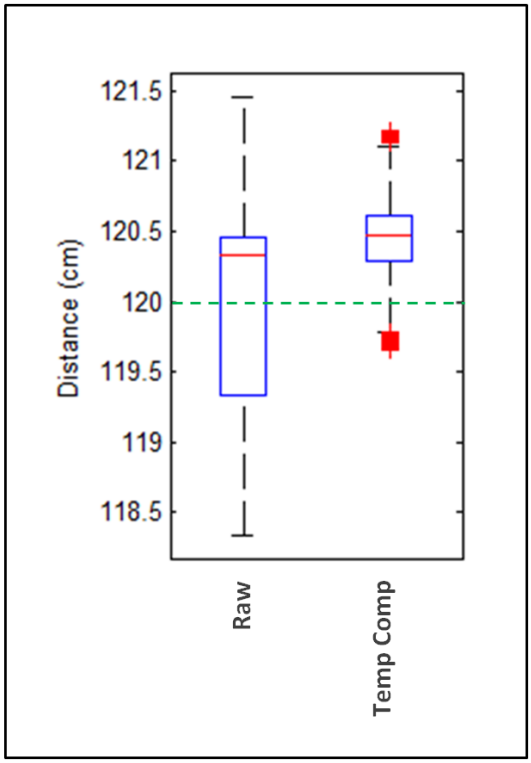

Figure 8 USD sensor performance verification test; box plots describing raw and air temperature compensated distributions of fixed target distance measurements obtained from a randomly selected USD sensor to assess both accuracy, precision, and the degree to which distance measurements are influenced by fluctuations in air temperature. Green line indicates actual target distance while the median, range of values with a 95 percent confidence interval, interquartile range (IQR), and outliers (outside the 95 percent confidence interval) are described by the red line, black whiskers, blue rectangle, and red cross, respectively.

3.1.3 USD Sensor Networks

Treeline USD Sensor Network

Treeline catchment can be described as sagebrush steppe ecotone with a classic symmetrical basin shape composed of opposing northeast and southwest slopes (between 10 and 35 degrees), all of which routes water to an ephemeral stream that leads to a single pour point (Figure 1). Table 2 identifies the location, aspect, slope, and vegetation classification of each USD sensor. Based on previous work by Jost et al. (2007), who identified aspect and vegetation type as key controls to local variability of snow water equivalent (SWE), five USD sensors were installed at Treeline catchment along a northeast to southwest transect (Figure 1). Including the Judd Communications snow depth sensor, USD sensors were located at upper, middle, and lower regions of both the northeast and southwest slopes at Treeline. Due to the proximity of the Treeline USD sensors to the site's existing power supply and data acquisition station, an alternative power supply and data acquisition scheme were implemented. The entire network was hardwired to the station's multiplexor connected to a Campbell Scientific CR-10X data logger, all of which collected voltage signals corresponding to snow accumulation and air temperature at 15 minute intervals. An example of the Campbell Scientific Edlog data acquisition program used for this study is included in Appendix C. The site's 12 volt power supply was composed of a deep cycle battery connected to a solar cell for recharging purposes.

Table 2 Treeline USD network specifications

Site	Northing (UTM 11N, NAD83)	Easting (UTM 11N, NAD83)	Slope (°)	Aspect (°)	Aspect Class	Vegitation Class	Sensor Elevation (cm above ground)
TLNE1	4842328	569240	10	44	North	Bare	177
TLNE2	4842305	569220	28	33	North	Shrub	150
TLSW3	4842336	569249	26	174	South	Shrub	175
TLSW4	4842347	569262	24	184	South	Shrub	165
TLSW5	4842364	569282	18	118	South	Shrub	158
TLJ	4842304	569250	22	40	North	Bare	120

Lower Deer Point USD Sensor Network

Lower Deer Point site is characterized as a ridge knob surrounded locally by shrubs and a mixed conifer forest. Here, consistent with findings by Jost et al. (2007), a randomized stratified pattern with respect to aspect and vegetation class was implemented for placement of the USD sensors. In all, 16 USD sensors were installed at Lower Deer Point in a randomized stratified pattern with respect to aspect and vegetation to reflect the nature of the site (Figure 10, Table 3). Each USD sensor was connected to a standalone 7 amp hour power supply and 4-channel U12 HOBO datalogger that collected voltage signals corresponding to snow accumulation and air temperature at 15 minute intervals (Figure 7). At installation sites with heavy ceanothus shrubs present, the USD sensor was placed above and pointed at the top of the shrubs. Previous field observations at Lower Deer Point during spring melt revealed all of the ceanothus shrubs and other bushes to be compressed downslope. This previous knowledge was investigated during the 2010 winter season, at which time a 1 m^2 area of the snow pack was excavated to expose the nature of the compressed ceanothus shrubs at a random location (Figure 9). The ceanothus was compressed and pointed downslope, which supports the notion that

both the weight of the snow pack and forces induced by downslope creep act to compress the shrubs to the base of the snow pack during the winter season.

Figure 9 Picture of ceanothus shrubs compressed below the snow pack at Lower Deer Point; area ceanothus shrubs are typically observed to be approximately 1 meter in height during late spring, summer and fall.

Table 3 Lower Deer Point USD network specifications

Site	Northing (UTM 11N, NAD83)	Easting (UTM 11N, NAD83)	Slope (°)	Aspect (°)	Aspect Class	Vegitation Class	Sensor Elevation (cm above ground)
LDP1	4843049	570702	8	127	South	Shrub	200
LDPE1	4843060	570728	22	84	East	Shrub	211
LDPE2	4843065	570752	28	88	East	Shrub	227
LDPE3	4843044	570802	20	88	East	Forest	205
LDPS1	4843024	570715	18	118	South	Shrub	213
LDPS2	4843003	570713	26	112	South	Shrub	220
LDPS4	4842981	570703	26	112	South	Shrub	215
LDPSE1	4843022	570748	24	84	East	Shrub	215
LDPSW4	4842966	570668	22	156	South	Shrub	189
LDPSW5	4842946	570663	22	164	South	Bare	177
LDPW1	4843062	570674	14	232	West	Shrub	212
LDPW2	4843055	570650	20	242	West	Shrub	211
LDPN1	4843253	570748	6	344	North	Shrub	244
LDPN2	4843436	570935	16	314	North	Forest	189
LDPJ	4843041	570694	7	190	South	Bare	220
HSD	4843271	571217	24	178	South	Forest	202
HND	4843438	570973	26	296	North	Forest	202

Figure 10 USD sensors and data acquisition at Lower Deer Point site

3.2 Determining Estimates of New Fallen SWE Accumulation

At any given site, SWE is equivalent to the product of the local bulk density and depth of snow (Jonas and Magnusson, 2009; Sturm et al., 2010). For this study, new fallen SWE associated with each precipitation event was estimated by Equation (3), where ρ_{ns} and h_{ns} are the density and accumulation of new fallen snow, respectively.

$$SWE = h_{ns}\rho_{ns} \quad (3)$$

To quantify the densities of new fallen snow at Treeline and Lower Deer Point, storm boards were placed at Treeline (Figure 1) and Lower Deer Point (Figure 2) to collect new fallen snow. Fourteen white HDPE storm boards were placed in a spatially stratified pattern with respect to site, aspect, and vegetation as illustrated in Figure 1 and Figure 2. New fallen snow density estimates for 9 precipitation events for each site were recorded. Within 6 hours after a snow precipitation event concluded, new fallen snow densities on the storm boards were determined using a Snowmetrics 12 inch SWE tube and scale (www.snowmetrics.com) as follows with the assumption that the basal layer was effectively incompressible and any down-slope movement of the snowpack was insignificant over the period of precipitation accumulation.

1. Insert tube into new fallen snow with vertical motion; where d_{tube} is the inside diameter of the SWE tube.
2. Record snow depth to nearest 2 mm increment (h_{ns}).
3. Hang SWE tube from scale hook to determine weight (w_{ns}).
4. Calculate new fallen snow density using Equation (2) (www.snowmetrics.com); where ρ_{ns} is new fallen snow density.
5. $\rho_{ns} = \frac{w_{ns}}{h_{ns}\pi r^2}$ (2)

New fallen snow densities obtained from all storm board locations are presented in Figure 11 and Figure 12. Box plots were selected to describe the variability because they allow both a qualitative and quantitative assessment of variability. With regards to the box plots presented in this report, the mean, median, range of values with a 95 percent confidence interval, interquartile range (IQR), and outliers (outside the 95 percent confidence interval) are described by the blue diamond, red line, black whiskers, blue rectangle, and red cross, respectively. The box plots in Figure 11 describe the variability associated with bulk new fallen snow density estimates relative to each precipitation event occurring during the 2011 winter season. Figure 12 describes the variability associated with all bulk new fallen snow density estimates occurring during the 2011 winter season lumped together. Since no storm board measurements were collected during the USD investigation period (2010 winter season), the distribution of lumped bulk new fallen snow density estimates appeared to better represent the general conditions that were likely to have occurred during the 2010 winter season. As such, basic statistics associated with the lumped bulk new fallen snow density estimates are included in Table 4. Review of Figure 12 and Table 4 supports the following: (1) The relatively low interquartile range of 0.04 g/cm^3 centered about the mean and median new fallen snow density values supports the validity of a single new fallen snow density estimate that is representative of conditions at both Treeline and Lower Deer Point sites. (2) A new fallen snow density value of 0.16 g/cm^3 is a reasonable estimate for both Treeline and Lower Deer Point sites. (3) Assuming a reasonable estimate of uncertainty as equivalent to one standard deviation, the uncertainty associated with the bulk new fallen snow density estimate is ±0.03 g/cm^3.

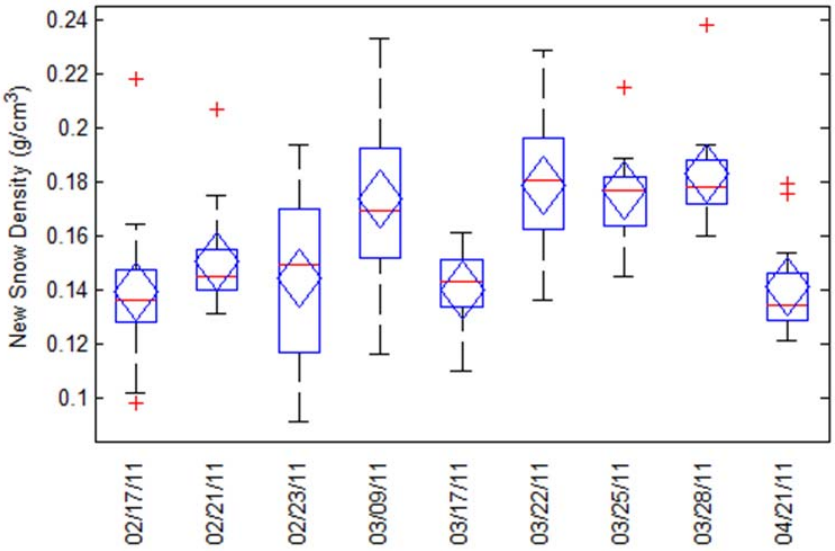

Figure 11 Box plot of new fallen snow density with respect to precipitation event; derived from storm board sample results collected during 9 precipitation events occurring during the 2011 winter season. The mean value, median, range of values with a 95 percent confidence interval, interquartile range (IQR), and outliers (outside the 95 percent confidence interval) are described by the blue diamond, red line, black whiskers, blue rectangle, and red cross, respectively.

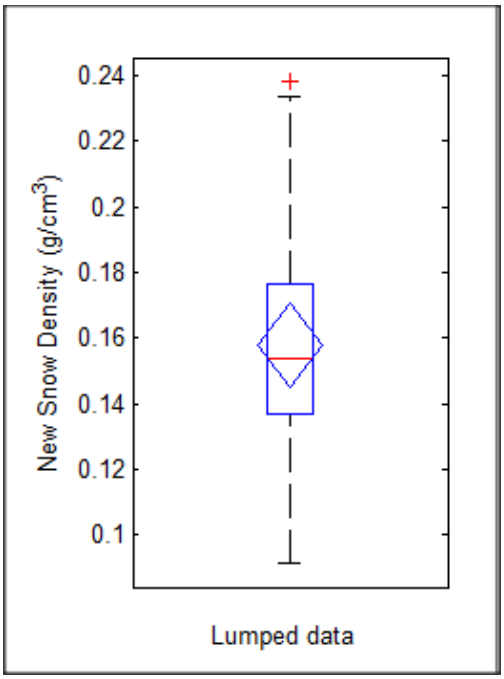

Figure 12 Box plot of lumped bulk new fallen snow density derived from storm board results; the lumped data set includes new fallen snow densities obtained from all storm board locations and storm events; derived from storm board sample results collected during 9 precipitation events occurring during the 2011 winter season

Table 4 Summary table describing variability associated with the lumped bulk new fallen snow density estimate based on sampling new fallen snow densities over the course of 9 precipitation events during the 2011 winter season as described in Section 3.2

Statistic	New Fallen Bulk Density
Range [g/cm^3]	0.15
Mean [g/cm^3]	0.16
Median [g/cm^3]	0.15
Std Dev	0.03
Varience	0.0009

CHAPTER 4: RESULTS

Snow precipitation events occurring on February 24, 2010, March 13, 2010, and March 30, 2010 were included as case studies for this investigation because all USD sensor sites (1) received snow accumulation on dense basal layer, (2) all USD sensor sites were operable with the exception of LDPE3, which appeared to have a faulty transceiver, and (3) air temperatures were below freezing prior to onset and during snowfall (Figure 13). Including only sites that experienced precipitation events while air temperatures were below 0 °C allowed for the assumption that the basal layer was effectively incompressible. Representative new fallen snow accumulation outputs obtained from the USD sensors are presented in Figures detailed in Section 4.1. Here, representative new fallen snow precipitation events from USD sensors located at north, east, south, and west aspects were overlaid to visually assess general temporal trends before, during, and after the snow precipitation event. The normalized new fallen snow accumulation totals were determined by identifying the height of the basal snow layer immediately prior to, and the height of the snow accumulation immediately following, each precipitation event using manual qualitative methods and subsequently taking the difference, which corresponds to the height of new fallen snow accumulation. Water accumulation obtained from site weighing-type precipitation bucket gauges was converted to effective snow accumulation for comparison purposes using the methods outlined in Section 3.2. Whereby, reported accumulation of water in the weighing-type bucket gauge was converted to centimeters of water then divided by the new fallen snow density estimate of 0.16 g/cm^3 to obtain an

effective estimate of new fallen snow depth. It is important to note that the water accumulation totals obtained from the Treeline and Lower Deer Point weighing-type precipitation gauges were not corrected for gauge-catch deficiencies.

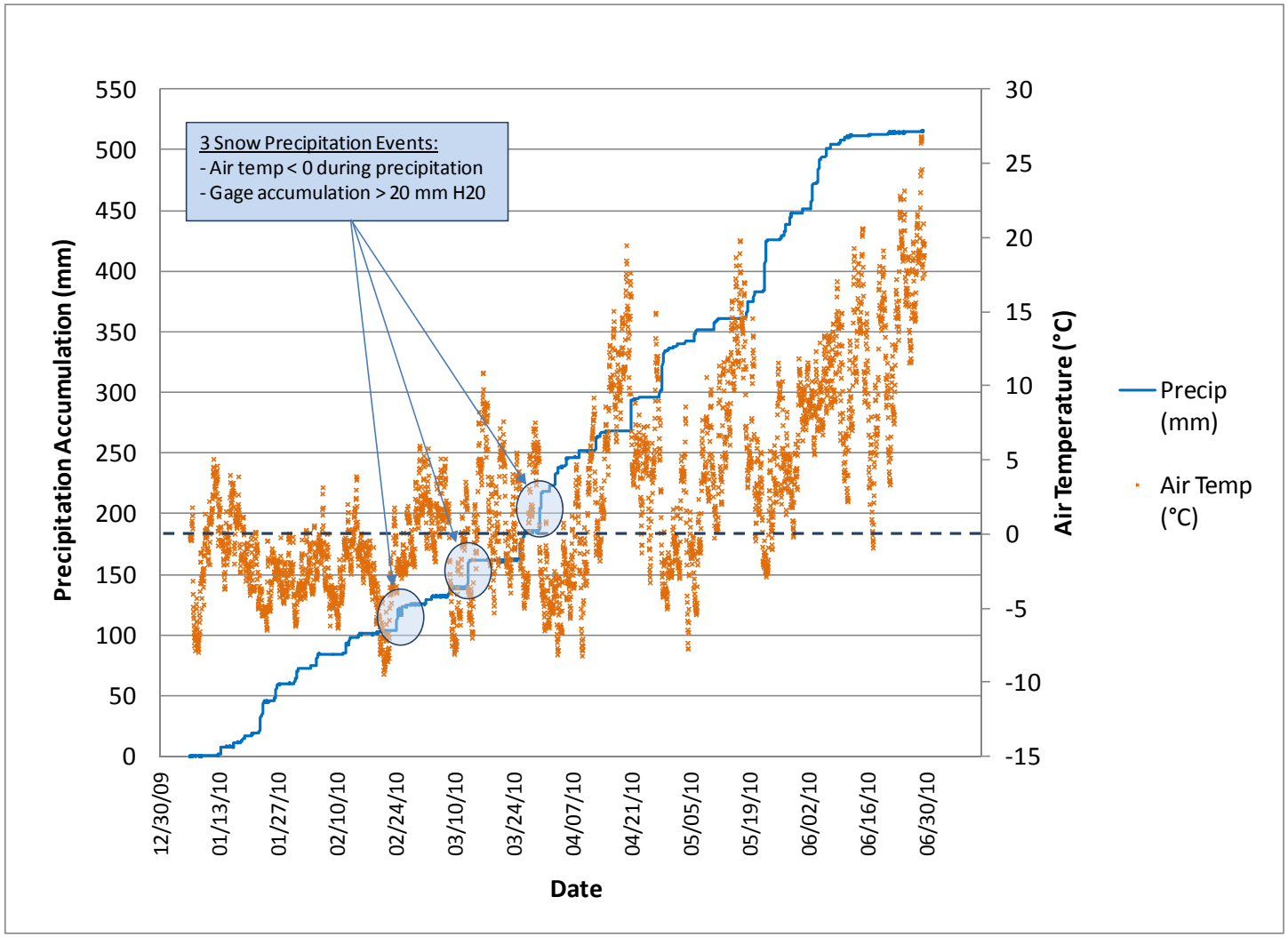

Figure 13. Precipitation accumulation during 2010 winter season at LDP

4.1 General Snow Precipitation Event Conditions

During the February 24, 2010 precipitation event, air temperature was below 0°C and wind speeds of 5 to +15 m/s were observed from the southeast at both Lower Deer Point and Treeline sites (Figure 14, Figure 15, and Figure 16). The dense and effectively incompressible basal layer assumption was supported by little previous snowpack densification before the storm, as the last precipitation event occurred 12 days earlier on February 12, 2010. Air temperature reached as high as 3.5°C with clear skies allowing full exposure to incoming solar radiation (Figure 15 and Figure 16) during the period of snowpack densification that occurred prior to the cold front and subsequent snow precipitation event on February 24, 2010. At Lower Deer Point, new fallen snow accumulation appeared consistent with bucket gauge observations (Figure 15). The range of new fallen snow accumulation was approximately 5 cm, centered about the bucket gauge observations. Sites located at wind shielded vegetation zones (LDPN1, LDPSE1, LDPS1) recorded larger snow depth changes snow than windward sites (LDPSW4, LDPW1), which all in turn recorded greater depth changes than the forested canopy sites (LDPN2). At Treeline, representative new fallen snow accumulation appeared more variable with respect to bucket gauge observations, likely influenced by the wind out of the southeast (Figure 14 and Figure 16) during snow precipitation. Ridge sites (TLNE1, TLSW5), with similar wind exposures, experienced similar accumulation of new fallen snow. Mid-slope sites with opposing northeast and southwest aspects (TLJ, TLSW4) appeared to experience moderate differential accumulation along with significant differences in densification and redistribution upon storm cessation (Figure 16). Opposing sites positioned near the base of the transect (TLNE2, TLSW3), approximately

15 feet up-gradient from the ephemeral channel, experienced similar new fallen snow accumulation. The range of new fallen snow accumulation was approximately 9 cm of snow depth.

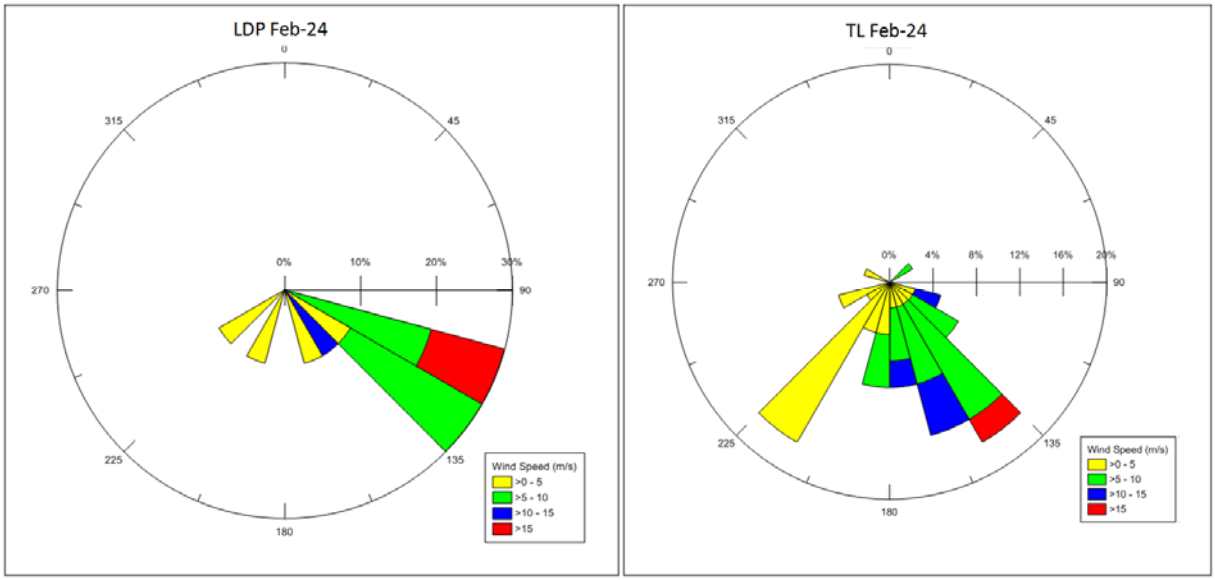

Figure 14 Wind rose diagram during February 24, 2010 precipitation event at Lower Deer Point (left) and Treeline (right).

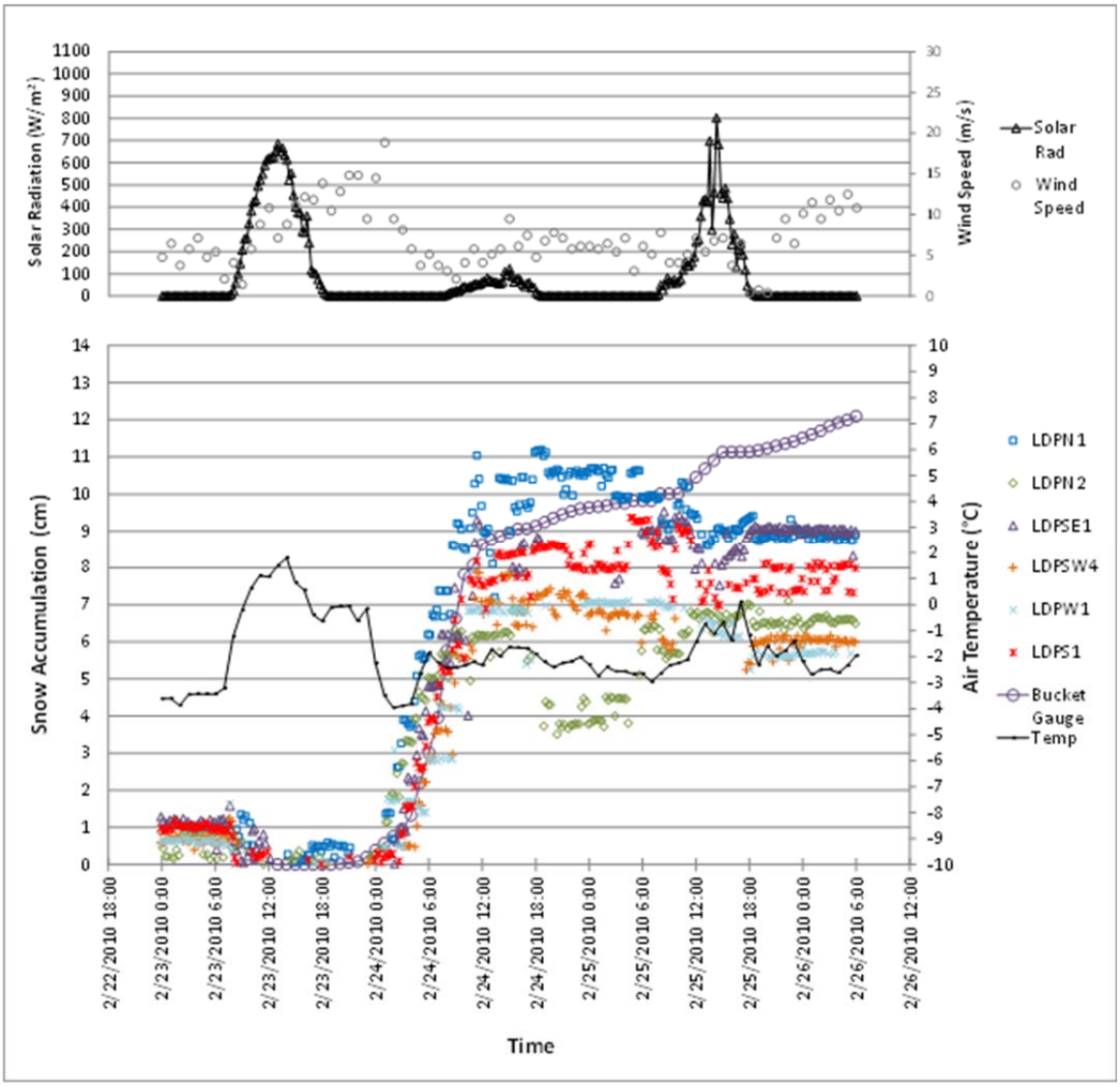

Figure 15 New fallen snow accumulation across representative USD sites at LDP on February 24, 2010; Overlaid with solar radiation, wind speed, air temperature and calculated effective snow accumulation as measured by the bucket gauge

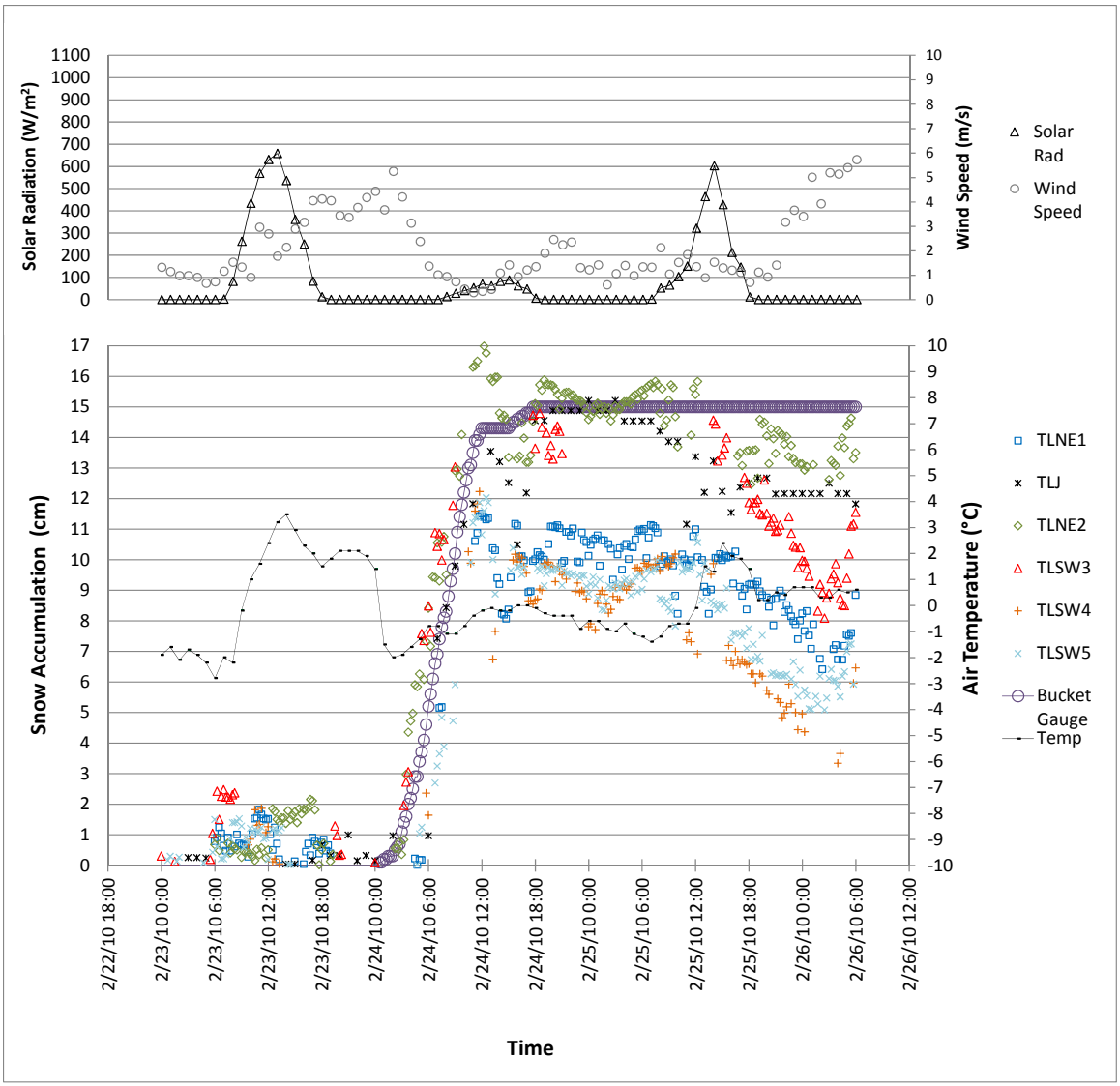

Figure 16 New fallen snow accumulation in depth across USD sites at TL on February 24, 2010; Overlaid with solar radiation, wind speed, air temperature and calculated effective snow accumulation as measured by the bucket gauge (converted to depth using a new snow density of 0.16 g/cm^3)

During the March 13, 2010 precipitation event, air temperature was below 0°C and wind speeds of 5 to +15 m/s were observed from the northwest from both Lower Deer Point and Treeline sites (Figure 17, Figure 18, and Figure 19). The dense and effectively incompressible basal layer assumption was supported by previous snowpack

metamorphism occurring since the last significant precipitation event on February 24, 2010 between which time there was light accumulation of snow on March 9, 2010. Air temperature reached as high as 7 °C with partially clear skies allowing for moderate exposure to incoming solar radiation (Figure 16) during the period of snowpack metamorphism that occurred prior to the cold front and subsequent snow precipitation event on March 13, 2010. At Lower Deer Point, representative new fallen snow accumulation appeared consistent with bucket gauge observations (Figure 18). All representative sites with the exception of LDPN1 and LDPW1 accumulated less snow depth than estimated from the bucket gauge, using a constant density of 0.16 g/cm^3.

Aspect and vegetation class controls on snow depth did not appear present. At Treeline, representative new fallen snow depth was highly variable, likely influenced by variability associated with wind speed and direction (Figure 17, Figure 18, and Figure 19), as well as variability in new snow density and densification rates. Aspect class controls did not appear present.

Twenty-four hours after storm cessation, all sites at Lower Deer Point and Treeline with a southern exposure experienced significant decline in apparent depth compared to sites with northern exposures. This decrease in depth appears to correlate strongly with exposure to solar radiation (Figure 18 and Figure 19), which leads to two potential explanations. Since snow temperature is one of the primary drivers of snowpack metamorphism, the decline in depth is potentially tracking densification of the newly formed snow layer, including the basal layer. An alternative explanation, albeit unlikely, would be that the change is depth is a result of lateral downslope movement of

the snowpack due to creep, a phenomenon that was inadvertently observed by the movement of caution flags marking USD sensor sites on occasion.

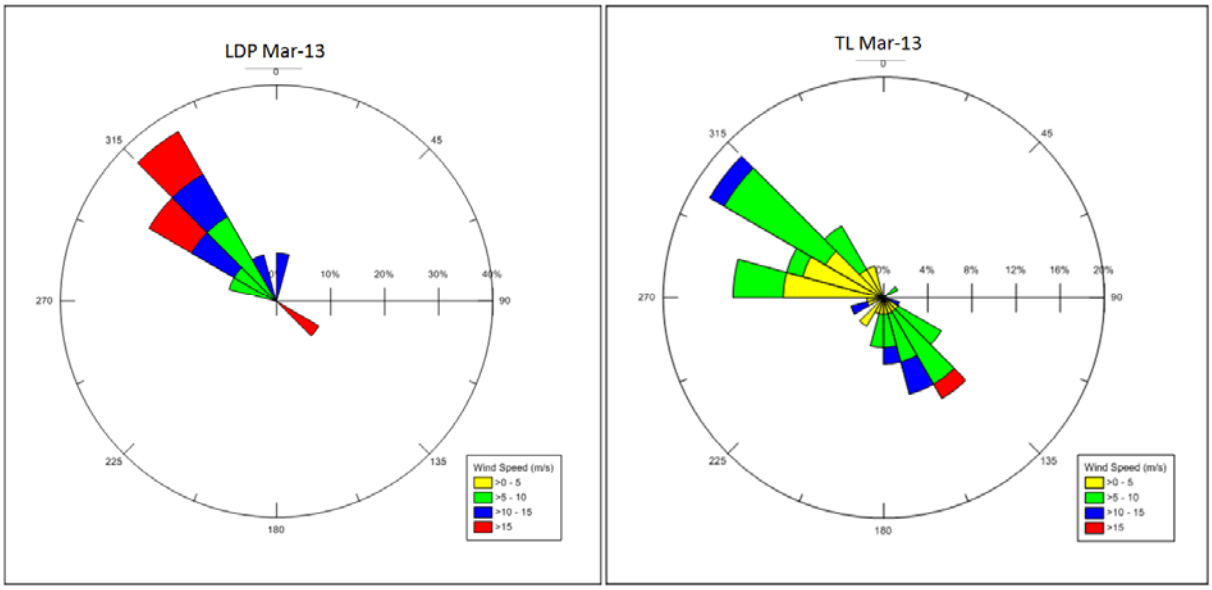

Figure 17 Wind rose diagram during March 13, 2010 precipitation event at Lower Deer Point (left) and Treeline (right).

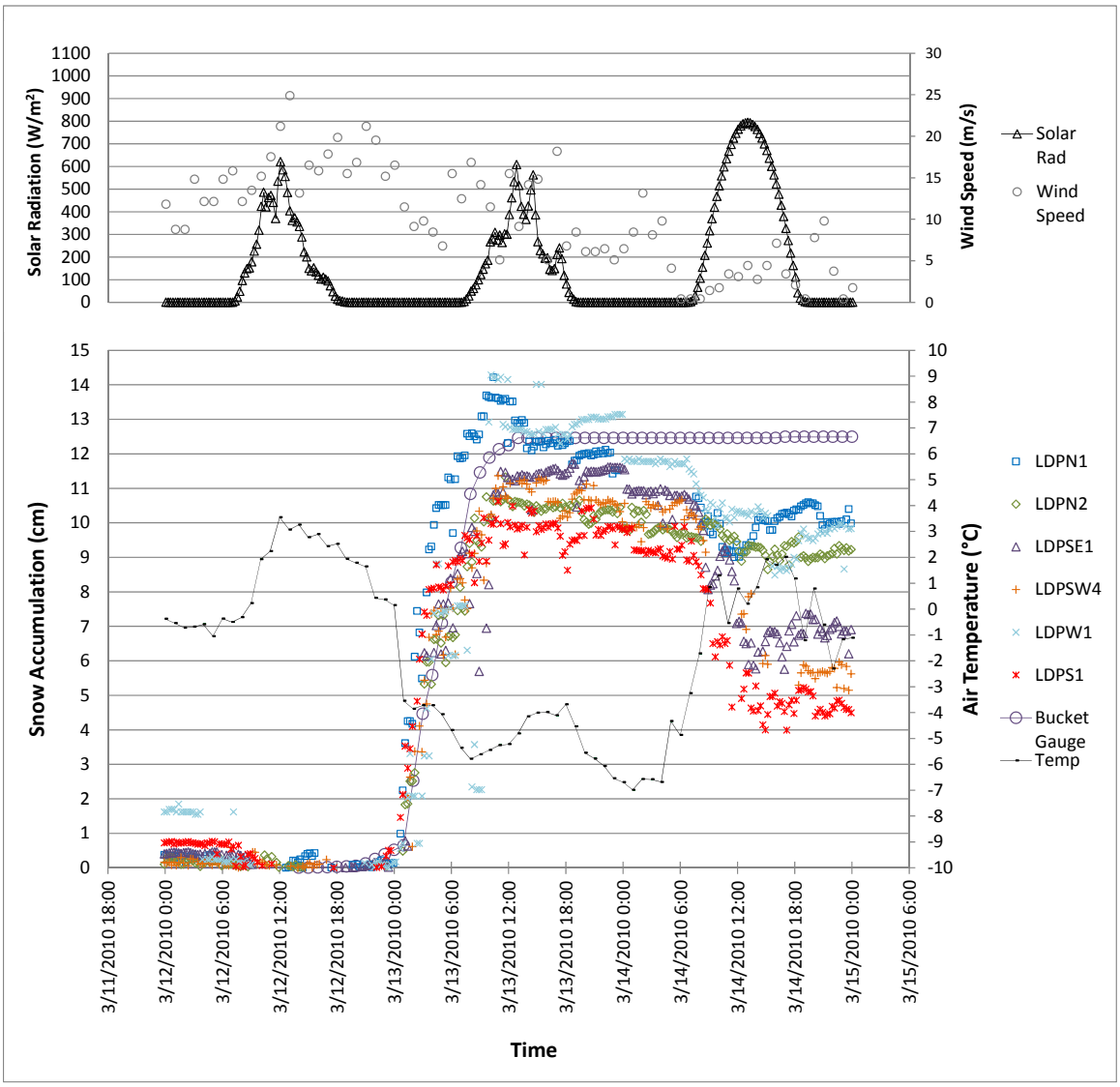

Figure 18 New fallen snow accumulation across representative USD sites at LDP on March 13, 2010; Overlaid with solar radiation, wind speed, air temperature and calculated effective snow accumulation as measured by the bucket gauge

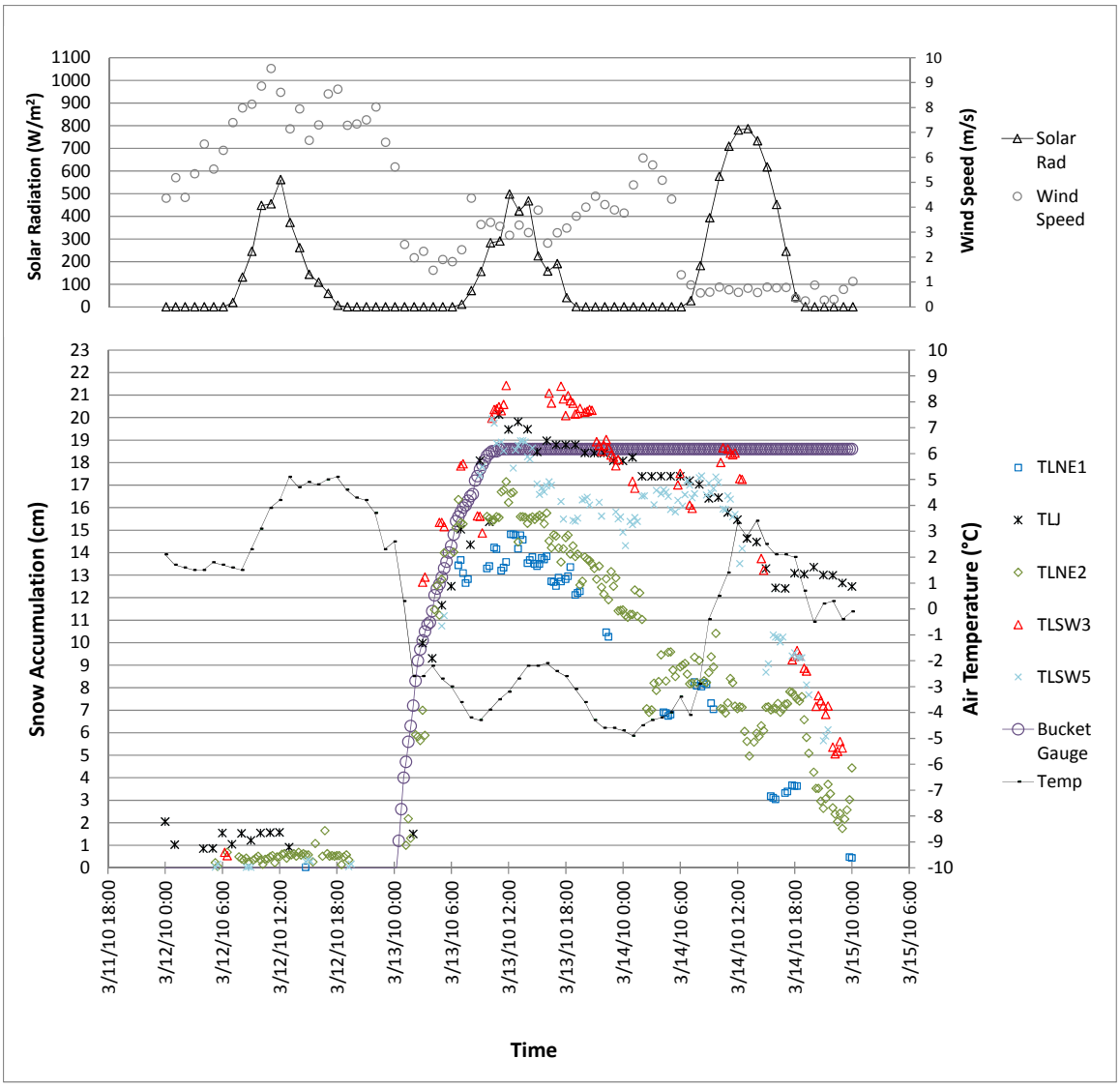

Figure 19 New fallen snow accumulation across USD sites at TL on March 13, 2010; Overlaid with solar radiation, wind speed, air temperature, and calculated effective snow accumulation as measured by the bucket gauge

During the March 30, 2010 precipitation event, air temperature was below 0°C and wind speeds of 5 to +15 m/s (Figure 20 and Figure 21) were observed from the west from both Lower Deer Point and Treeline sites. The dense and effectively incompressible basal layer assumption was supported by little previous snowpack metamorphism prior to the storm, due to the last significant precipitation event 5 days before on March 25, 2010.

Air temperature reached as high as 8 °C during the period of snowpack densification that occurred prior to the cold front and subsequent snow precipitation event on March 30, 2010. As illustrated in Figure 19, representative new fallen snow accumulation was highly variable, likely influenced by the higher sustained wind speeds that originated out of the west (Figure 20 and Figure 21). During the latter 2 hours of the snow accumulation period, average hourly wind speeds were 19.5 and 16.5 m/s, respectively. Sites located at wind shielded vegetation zones (LDPN1, LDPSE1, LDPS1) accumulated significantly more snow depth than LDPSW4 (exposed to wind) and LDPN1 (forested canopy). Additionally, the variable nature of snow accumulation is highlighted by observed differences between LDPW1 and LDPSW4 wind exposed sites, with snow accumulations of 24.0 cm and 14.5 cm depth respectively. As observed during the March 13, 2010 event, 18 hours after storm cessation a significant decline in accumulated snow depth appears to correlate strongly with exposure to incoming solar radiation (Figure 19).

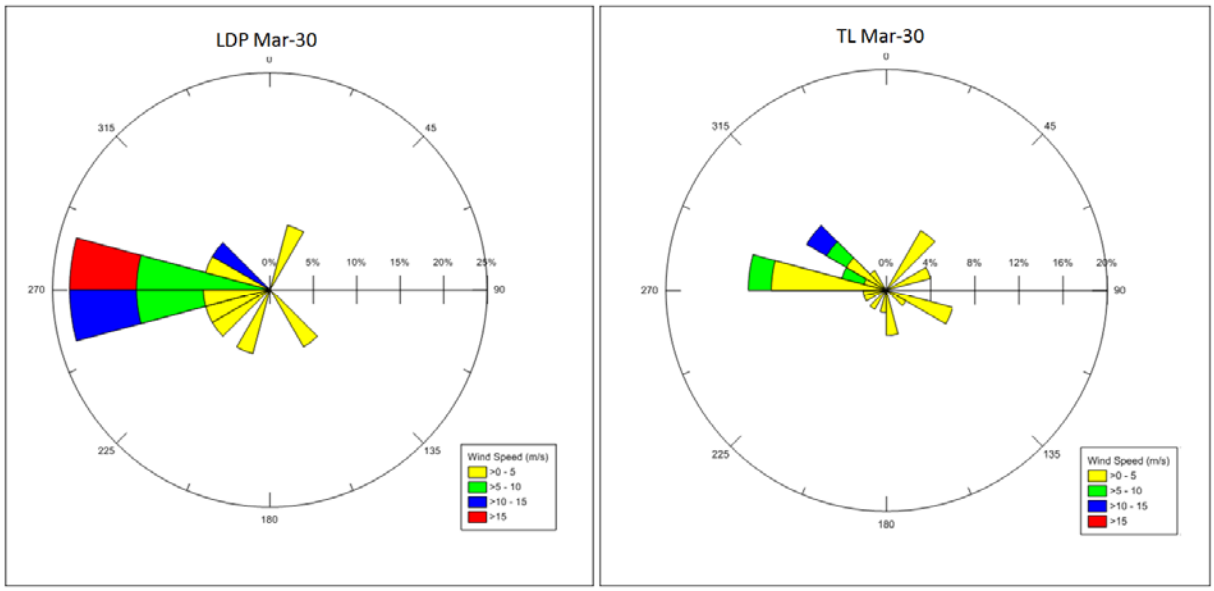

Figure 20 Wind rose diagram during March 30, 2010 precipitation event at Lower Deer Point (left) and Treeline (right).

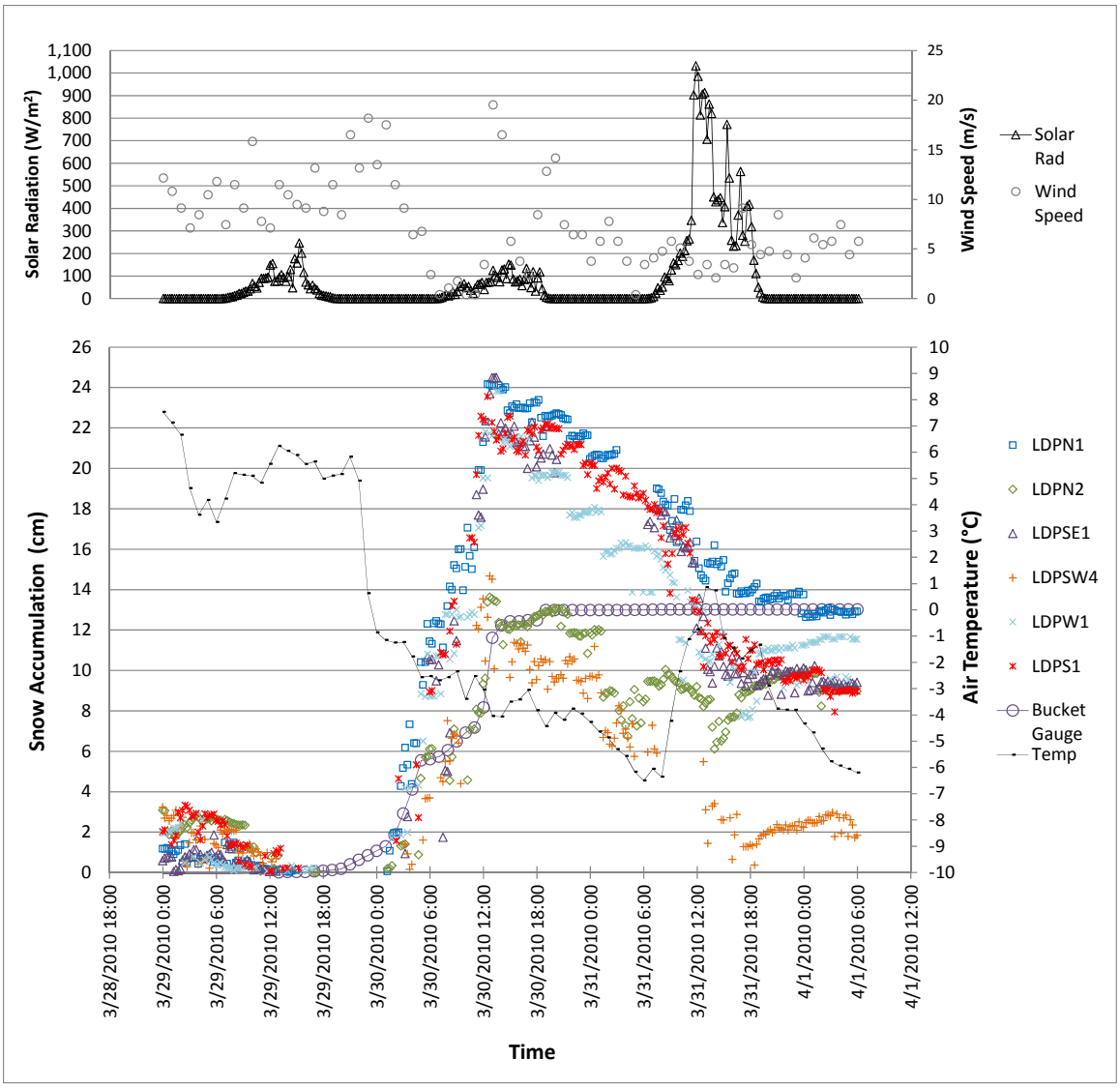

Figure 21 New fallen snow accumulation across representative USD sites at LDP on March 30, 2010; Overlaid with solar radiation, wind speed, air temperature and calculated effective snow accumulation as measured by the bucket gauge

4.2 Local Variability at Lower Deer Point

USD sensor installation locations at Lower Deer Point followed a randomized stratified pattern with respect to aspect and vegetation class (Figure 2). Box plots describing lumped new fallen SWE variability with respect to precipitation gauge measurements at Lower Deer Point are presented in Figure 22 and Table 5. Here snow

depth change is converted to new SWE using a density of 0.16 g/cm^3, in contrast to previous figures that were given in terms of snow depth. Review of accumulation distributions supported the notion that vegetation type was by far the most significant controlling mechanism for new fallen SWE distributions discussed by Jost et al. (2007). As a result, new fallen SWE accumulation data was partitioned into three classifications:

- ***Bare***: sites characterized by compressed shrubs (below the snowpack) and significant exposure.
- ***Vegetation transition***: sites characterized by compressed shrubs (below the snowpack) and bordering heavy distributions of large exposed shrubs and mixed conifer forested areas.
- ***Canopy***: sites located within the mixed conifer forest and below a dense canopy.

Figure 23 presents box plots corresponding to new fallen SWE accumulation with respect to vegetation class for the Lower Deer Point sites all of which is compared to bucket gauge observations for each precipitation event. While differences in magnitude can be observed between each precipitation event, a clear trend based on vegetation class appears present. (1) Vegetation transition sites experienced the highest accumulation with the lowest variability. (2) Bare sites experienced moderate accumulation with the highest variability. (3) Canopy sites generally experienced the lowest accumulation with moderate variability. Table 5 describes the SWE variability at Lower Deer Point for each precipitation event. Variation within class and differences between estimated SWE from depth observations and precipitation observations are likely due to variations in new snow density and densification rates. However, while this study did not reveal any significant trends in measured density, we can estimate the uncertainty associated with

our bulk new fallen snow density estimate (Table 4). Assuming one standard deviation as a reasonable estimate of uncertainty, uncertainty associated with bulk new fallen snow density (Table 4), along with uncertainty associated with our new fallen snow accumulation can be propagated through Equation 3 using Equation 4 (Holman, 2001; Potter et al., 2010) to determine uncertainty associated with calculated SWE estimates presented in Table 5.

$$\Delta SWE = \overline{SWE} * \sqrt{\left(\frac{\Delta h_{ns}}{\bar{h}_{ns}}\right)^2 + \left(\frac{\Delta \rho_{ns}}{\bar{\rho}_{ns}}\right)^2} \quad (4)$$

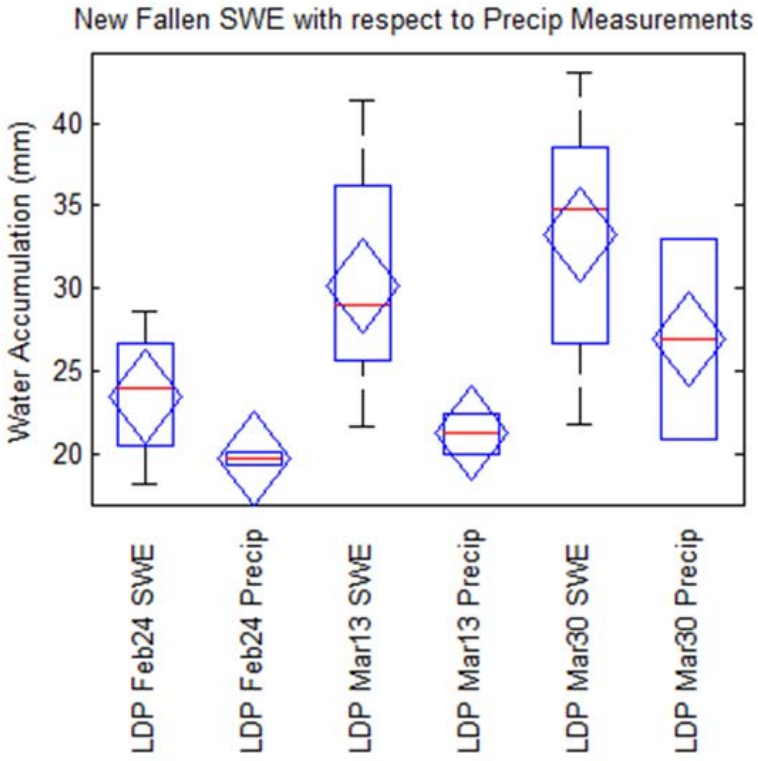

Figure 22 Box plots of new fallen SWE with respect precipitation measurements at Lower Deer Point. With regards to the box plots, the mean value, median, range of values with a 95 percent confidence interval, interquartile range (IQR), and outliers (outside the 95 percent confidence interval) are described by the blue diamond, red line, black whiskers, blue rectangle, and red cross, respectively.

Table 5 Summary table describing new fallen SWE variability at LDP site

Statistic	Feb-24	Mar-13	Mar-30
Range [mm H_2O]	10.5	19.7	21.2
Mean [mm H_2O]	23.5	30.1	33.3
Median [mm H_2O]	24.0	29.0	34.8
Std Dev [mm H_2O]	3.6	6.0	6.9
Varience	13.1	35.6	47.9
Mean Precip Bucket Accum [mm H_2O]	19.7	21.2	26.9
Uncertainty [mm H_2O]	4.4	5.7	6.3

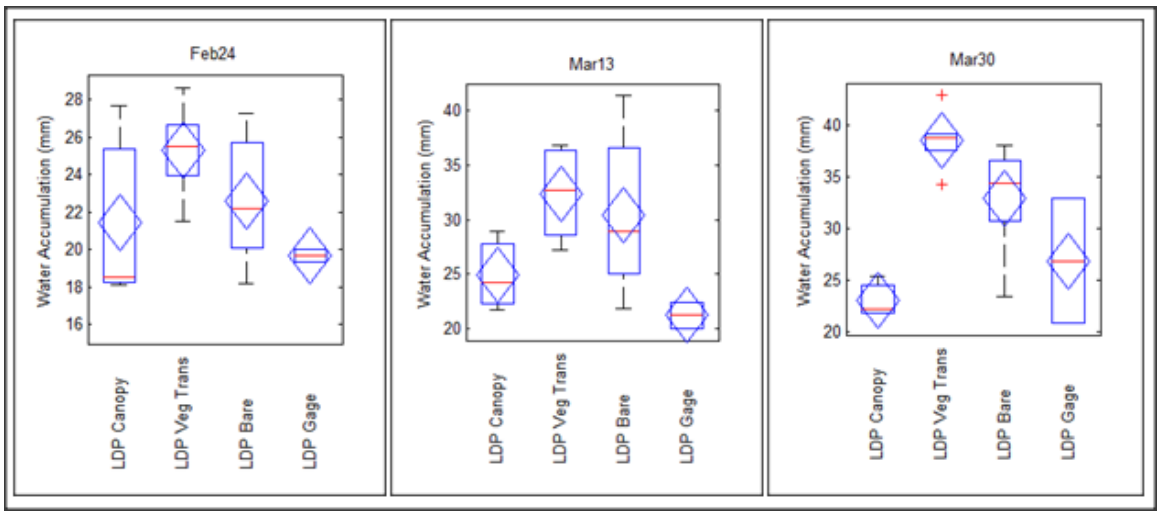

Figure 23 Box plots corresponding to new fallen estimated SWE accumulation, using a constant density, with respect to vegetation class for LDP sites

4.3 Local Variability at Treeline

USD sensor installation locations at the Treeline followed a northeast to southwest transect of the catchment. Treeline USD sensors effectively captured upper, middle, and lower regions of both the northeast and southwest slopes at Treeline. Box plots describing lumped new fallen SWE variability (uncertainty) with respect to precipitation gauge measurements at Treeline are presented in Figure 24 and Table 6.

Due to the homogeneous nature of the vegetation class, composed nearly entirely of sagebrush and other small shrubs, aspect appeared to be the primary mechanism controlling accumulation of new fallen SWE. As a result, new fallen SWE accumulation data was partitioned into two classifications:

- ***North***: sites characterized by sagebrush and other small shrubs with northeast exposures.
- ***South***: sites characterized by sagebrush and other small shrubs with southwest exposures.

Figure 24 presents box plots corresponding to new fallen SWE accumulation with respect to aspect for Treeline sites all of which are compared to on-site weighing-type bucket gauge observations for each precipitation event. While differences in magnitude can be observed between each precipitation event, no clear trend based on aspect appears present. Likely depending on wind speed and direction, accumulation was more or less consistent on north and south aspects, both of which accumulated more water than observed in the weighing-type bucket gauges. Density and densification rate variations could explain differences. Table 6 describes the SWE variability at Treeline for each precipitation event. Variation within class and differences between estimated SWE from depth observations and precipitation observations are likely due to variations in new snow density and densification rates. However, while this study did not reveal any significant trends in measured density, we can estimate the uncertainty associated with our bulk new fallen snow density estimate (Table 4). Assuming one standard deviation as a reasonable estimate of uncertainty, uncertainty associated with bulk new fallen snow density (Table 4), along with uncertainty associated with our new fallen snow

accumulation can be propagated through Equation 3 using Equation 4 (Holman, 2001) to determine uncertainty associated with calculated SWE estimates presented in Table 6.

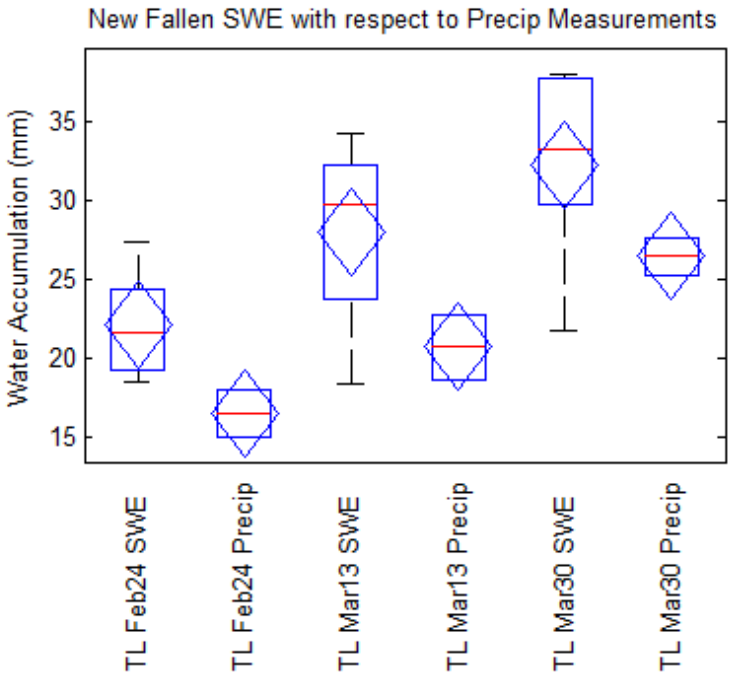

Figure 24 Box plots of new fallen SWE with respect precipitation measurements at Treeline. With regards to the box plots, the mean value, median, range of values with a 95 percent confidence interval, interquartile range (IQR), and outliers (outside the 95 percent confidence interval) are described by the blue diamond, red line, black whiskers, blue rectangle, and red cross, respectively.

Table 6 Summary table describing new fallen SWE variability at TL site

Statistic	Feb-24	Mar-13	Mar-30
Range [mm H_2O]	8.9	16.0	16.3
Mean [mm H_2O]	22.1	28.0	32.3
Median [mm H_2O]	21.6	29.7	33.3
Std Dev [mm H_2O]	3.5	6.1	6.4
Varience	12.6	37.0	40.9
Mean Precip Bucket Accum [mm H_2O]	16.5	20.7	26.4
Uncertainty [mm H_2O]	4.2	5.3	6.1

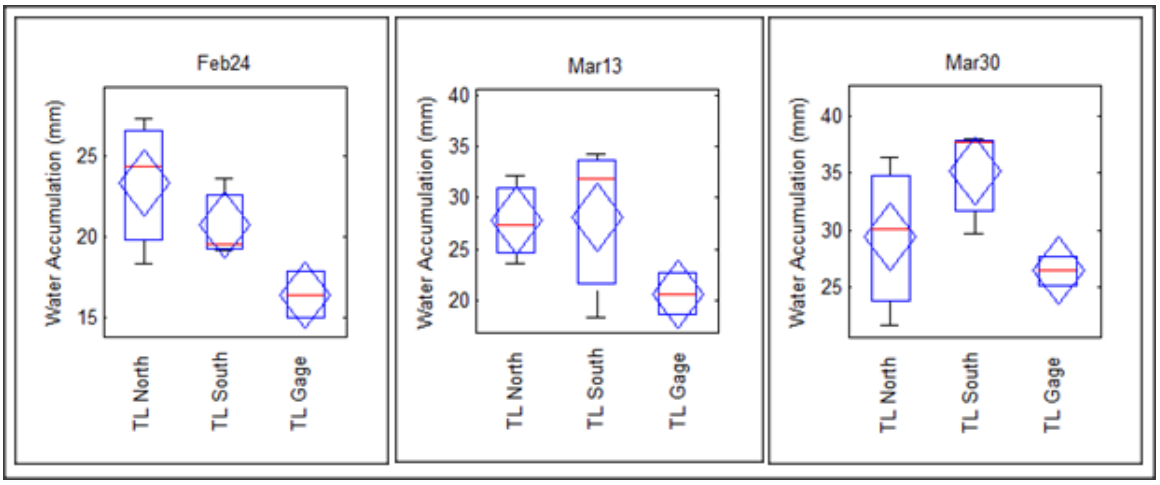

Figure 25 Box plots corresponding to new fallen estimated SWE accumulation, using a constant density, with respect to aspect for TL sites

CHAPTER 5: DISCUSSION

5.1 The Inexpensive USD Sensor

Overall, the inexpensive USD sensors developed and constructed for this study performed quite well, all things considered. The USD sensors provided performance characteristics that were consistent with those advertised for commercially available alternatives, attaining an accuracy (bias) within 0.5 cm and a precision of less than 0.32 cm (defining precision as one standard deviation) when tested above a flat concrete slab over the temperature range of 0 to 10 °C. Any future work using these USD sensors should consider the following:

1. During site installation, the USD sensor and internal XL-MaxSonar EZ-2 transceiver needs to be positioned normal to the surface of the snow. The transceiver is very sensitive to interference from either the ground or internal cover, so it is critical that it is tested in the field prior to leaving the site. Physically adjusting the sound pulse direction of the USD sensor or internal transceiver was required at most sites to obtain a true depth signal.
2. Additionally, selection of each USD installation site poses many challenges, and any decisions must be based on the question one is trying to answer. As with any USD sensor, the measurement target (i.e., ground surface or snow surface) must be clear of any rocks, sticks, or branches

that might interfere with the signal from the USD. So when installing USD sensors at a densely vegetated area such as Lower Deer Point, one can either remove all vegetation, rocks, and sticks from the measurement target and rake it flat or simply point the USD sensor at the top of the vegetation. For this study, we selected the latter method. Removing vegetation is no trivial task, and while it does allow for continuous measurement of snow accumulation through the entire winter season, the act appeared to effectively create a vegetation transition site that would catch redistributed snow. Since we were interested in new fallen snow accumulation, not season total, merely pointing the USD sensor towards the ground and at the vegetation sufficed. We found that as soon as the snowpack forms, smaller shrubs such as ceanothus that are less than approximately 1 meter in height were compressed below the snowpack and pointed downslope as described in Section 3.1.3.

3. The USD sensors collect raw, so-called zero order data that is quite noisy. There is no optimized internal algorithm as seen in commercially available alternatives that clean the data. As a result, manual and qualitative techniques were required to remove outliers associated with our dataset that was collected at 15 minute intervals. It is highly recommended to collect measurements at 1 minute intervals, as the larger dataset greatly improves post processing capabilities by enabling the ability statistically distinguish random and non-random variability.

5.2 Local Variability with Respect to Site Precipitation Gauge Observations

The purpose of this study was to assess local variability of water accumulation in the form of new fallen snow with respect to site precipitation gauge observations using a network of inexpensive USD sensors. Comparing observed variability between Treeline and Lower Deer Point over the course of each storm (Figure 22 and Figure 24, Table 5 and Table 6) found that (1) measures of variability such as range and standard deviation for both locations were more or less the same and (2) variability increases at both locations with increasing snow accumulation. These findings are consistent with what Ryan et al. (2008b) noticed at the 17 NWS-ASOS sites, which were outfitted with 3 USD sensors at each site.

Controls on snow accumulation at a small catchment in a sagebrush steppe ecotone (Treeline) are quite different than that at a ridge knob with a mixed shrubs and conifers (Lower Deer Point). At Lower Deer Point, while differences in the magnitude of snow accumulation can be observed between each precipitation event, a clear trend based on vegetation class appears present (Figure 23). (1) Vegetation transition sites, those with mixed shrubs and bordering conifer forests, experienced the highest snow accumulation with the lowest variability. (2) Bare sites, with shrubs compressed at the base of the pack, experienced moderate snow accumulation with the highest variability. (3) Canopy sites generally experienced the lowest snow accumulation with moderate variability. With respect to precipitation events occurring on February 24, March 13, and March 30 at Lower Deer Point, weighing-type precipitation gauge underestimates (gauge-catch deficiencies) were approximately 16%, 30%, and 19%, respectively. However, it is important to note that these percent gauge-catch deficiencies contain

significant uncertainty themselves. Uncertainty estimates of SWE at Lower Deer Point (Table 5) suggest that the calculated gauge-catch deficiencies have percent uncertainties of ±19%. At Treeline, while differences in the magnitude of snow accumulation can be observed between each precipitation event, no clear trend based on aspect appears present (Figure 25). Likely depending on wind speed and direction, accumulation was more or less consistent on north and south aspects. With respect to precipitation events occurring on February 24, March 13, and March 30 at Treeline, weighing-type precipitation gauge underestimates (gauge-catch deficiencies) were approximately 26%, 26%, and 18%, respectively. However, as described for Lower Deer Point above, it is important to note that these percent gauge-catch deficiencies contain significant uncertainty themselves. Uncertainty estimates of SWE at Treeline (Table 6) suggest that the calculated gauge-catch deficiencies have percent uncertainties of ±19%.

5.3 Hydrologic Significance and Potential Uses for Inexpensive Ultrasonic Snow Depth Senor Networks

Precipitation measurement uncertainty is commonly regarded as an important factor influencing model performances but rarely quantified (Larson and Peck 1974; Peck, 1997; Yang et al., 2000; Slater and Clark, 2006; Harmel and Smith, 2007). Findings from this study suggest that networks of ultrasonic snow depth sensors can successfully be used to assess and quantify the variability associated with snow precipitation gauge observations at meteorological sites.

5.3.1 Generating Uncertainty Estimates for Operational Hydrologic Models

The National Weather Service (NWS) stresses the importance and challenges researchers to develop methods by which error estimates can be added to streamflow predictions generated by operational hydrologic models (personal communication, Dr. Pedro Restrepo of the NWS Office of Hydrologic Development Hydrology Laboratory). Findings from this study suggest that, in snow dominated catchments, setting up a network of USD sensors around meteorological stations can provide value added information with regards to error estimates. More specifically, using the methods outlined above, water accumulation estimates obtained from USD networks placed around meteorological sites enable direct determination of uncertainty estimates associated with standard precipitation observations such as those obtained from weighing bucket gauges. Subsequent uncertainty estimates, similar to those presented in this study, can then be propagated through the hydrologic model, enabling placement of error bars on output estimates.

5.3.2 Generating Improved Uncertainty Estimates of Observationally Derived Precipitation Data at the Watershed Scale

To improve error estimates at the basin scale, methods of determining optimal locations of USD sensor networks is imperative to ensure propagation of a basin-wide representative distribution. One such method, presented by Shallcross et al. (2010), involved the determination of site specific controls on the spatial distribution of snow. The study utilized airborne LiDAR (Light Detection And Ranging) combined with a binary regression tree model to identify a handful of statistically significant discrete grid cells that effectively characterize Dry Creek Experimental Watershed. Placement of

USD sensor network clusters at these locations would enable field based variability estimates that are more reflective of the watershed.

5.3.3 Incorporating USD Network Precipitation Measurements with Data Assimilation Methodologies

Use of data assimilation methods to improve streamflow forecast model simulation estimates has been increasing (Houser et al., 1998; Reichle et al., 2002; Slater and Clark, 2006; Clark et al., 2006). Common adaptive methods of data assimilation such as the Kalmen Filter (EKF) or Ensemble Kalmen Filter (EnKF) have the potential to benefit greatly from observational snow precipitation data sets obtained from USD sensor networks.

EKFs utilize a linear model to propagate errors associated with model state variables forward in time (Slater and Clark, 2006). Since determination of the required grid cell variances and subsequent covariances using Monte Carlo or iterative methods is no trivial task, a field based option can now be considered. Assuming a standard 30 meter model grid cell size, networks of 10 USD sensors placed in random locations within a 15 meter radius of area meteorological stations would provide a distribution of observational snow depth data. This distribution could be used to explicitly determine estimates of variance and subsequent covariance associated with the 30 meter grid cell, which in turn could be incorporated directly into the ENK model. Similarly, this scheme could be applied to EnKF models. EnKFs are similar to ENKs with the exception that they utilize ensembles of randomly generated data for each grid cell to inherently carry error estimates forward in time (Slater and Clark, 2006). Each grid cell ensemble is

generated based on estimates of variance, which much like in EKFs, could benefit from using observationally derived data sets to describe the ensemble distributions.

5.4 Impact of Solar Radiation on New Fallen Snow Metamorphism

Metamorphism or densification of a new fallen snow layer is driven by energy exchanges occurring at the interface between the snowpack and the atmosphere (Armstrong and Brun, 2008). The governing energy balance is driven by shortwave (solar) radiation, longwave radiation, sensible heat, latent heat, and to a lesser extent from energy fluxes associated with mass transfer from blowing snow and conduction from the basal layer (Armstrong and Brun, 2008). Above all sources of energy, solar radiation appeared to have significant influence on the rate of densification at both Lower Deer Point and Treeline sites. This was evident by a shift down in the normalized depth of the new fallen snow layer at sites characterized by a southern exposure (Figure 18 and Figure 19). Upon cessation of the March 13, 2010 precipitation event, densification of the new fallen snow layer appeared comparable across all USD sensors at Lower Deer Point and Treeline sites until reaching what could be effectively described as a cliff (shift down) in the apparent depth of the new fallen snow layer. Weather conditions leading to the observed shift at USD sites with southern aspects could be described as having cool temperatures, clear skies, and low wind. At Lower Deer Point, air temperatures were less than 2°C, wind speeds less than 4 m/s and solar radiation reached approximately 800 W/m^2 over the course of a smooth diurnal cycle, which indicates clear and sunny conditions were present throughout the day. At Treeline, air temperatures were less than 4.5°C, wind speeds less than 2 m/s, and solar radiation reached approximately 790 W/m^2 over the course of a smooth diurnal cycle, which indicates clear and sunny conditions

were present throughout the day. The low wind and cool air temperatures would suggest that the impact of sensible and latent heat exchanges were minimal, while the lack of cloud cover eliminates any significant influx of longwave radiation. All of which leads to the conclusion that incoming solar radiation causing increased snow temperature is likely the cause of the accelerated rate of densification of the new fallen snow layer.

The alternate hypothesis that the shift down in apparent new fallen snow depth is a result of lateral downslope movement of the snowpack due to creep is unlikely for a few reasons. (1) While creep was documented in the field by observed movements in caution flags around USD sensor sites along with compressed ceanothus shrubs pointed downslope, significant movements of the snowpack were only observed during warmer spring time conditions at exposed sites characterized with steep slopes. (2) LDPSE1 was one of the USD sites with a southern aspect that experienced a shift down in snow depth. LDPSE1 has a relatively low slope and is located at a vegetation transition site that boarders a heavy distribution of large exposed shrubs and a mixed conifer forested area located downslope and to the north. These conditions would tend to inhibit the occurrence of creep. (3) Solar radiation can penetrate up to 10 cm into the snowpack (Armstrong and Brun, 2008), which would alone suggest a significant influence on the densification of a new fallen snow layer of approximately 12 cm.

CHAPTER 6: CONCLUSIONS

The purpose of this study was to investigate local variability of SWE in the form of new fallen snow and develop uncertainty estimates to assess how well data obtained from standard precipitation gauges represents local conditions using a network of ultrasonic snow depth sensors. USD sensor networks at Lower Deer Point and Treeline research sites were used to collect snow accumulation time series' over the course of the 2009-2010 winter season. During this period, three specific snow precipitation events occurring on February 24, 2010, March 13, 2010, and March 30, 2010 were included as case studies in this investigation. The findings of the investigation are as follows.

At Lower Deer Point, spatial topographic, and vegetation class controls on new fallen SWE accumulation appear present. As described in Figure 23, vegetation transition sites experienced the highest accumulation with the lowest variability, bare sites experienced moderate accumulation with the highest variability, and canopy sites generally experienced the lowest accumulation with moderate variability. With respect to precipitation events occurring on February 24, March 13, and March 30, weighing-type precipitation gauge underestimates (gauge-catch deficiencies) were approximately 16%, 30%, and 19%, respectively. However, it is important to note that these percent gauge-catch deficiencies contain significant uncertainty themselves. Uncertainty estimates of SWE at Lower Deer Point (Table 5) suggest that the calculated gauge-catch deficiencies have percent uncertainties of ±19%.

At Treeline, spatial topographic controls on new fallen SWE accumulation are inconclusive. Accumulation at Treeline site was more or less consistent on both north and south aspects and appeared to be controlled by wind speed and direction. While controls on accumulation could not be explicitly identified, the variability observed during each precipitation event was consistent (Figure 25). With respect to precipitation events occurring on February 24, March 13, and March 30 at Treeline, weighing-type precipitation gauge underestimates (gauge-catch deficiencies) were approximately 26%, 26%, and 18%, respectively. However, as described for Lower Deer Point above, it is important to note that these percent gauge-catch deficiencies contain significant uncertainty themselves. Uncertainty estimates of SWE at Treeline (Table 6) suggest that the calculated gauge-catch deficiencies have percent uncertainties of ±19%.

CHAPTER 7: REFERENCES

Anderson BT. 2011. Spatial Distribution and Evolution of a Seasonal Snowpack in Complex Terrain: An Evaluation of the SNODAS Modeling Product. In: Department of Geosciences, Boise State University.

Anderson EA. 1973. National Weather Service River Forecast System - Snow Accumulation and Ablation Model. Service NW (ed.).

Armstrong RL, Brun E, 2008. Snow and Climate. Cambridge University Press.

Burnop AC. 2012. Assessing the Value of Improved Snow Information in Operational Hydrologic Models. In: Department of Geosciences, Boise State University.

Clark MP, Slater AG. 2006. Probabilistic quantitative precipitation estimation in complex terrain. Journal of Hydrometeorology, **7**: 3-22.

Clark MP, Slater AG, Barrett AP, Hay LE, McCabe GJ, Rajagopalan B, Leavesley GH. 2006. Assimilation of snow covered area information into hydrologic and land-surface models. Advances in Water Resources, **29**: 1209-1221.

Dingman SL. 2008. Physical Hydrology. 2nd Edn., Waveland Press, Inc.

Eiriksson D. 2012. The Hydrologic Significance of Lateral Water Flow in Snow. In: Department of Geosciences, Boise State University.

Fassnacht SR. 2004. Estimating Alter-shielded gauge snowfall undercatch, snowpack sublimation, and blowing snow transport at six sites in the coterminous USA. Hydrological Processes, **18**: 3481-3492.

Goodison BE. 1978. Accuracy of Canadian Snow Gauge Measurements. Journal of Applied Meteorology, **17**: 1542-1548.

Goodison BE, Metcalfe J, Wilson B, Jones K. 1988. The Canadian Automatic Snow Depth Sensor: A Performance Update. In: 56th Annual Western Snow Conference.

Goodison BE, Wilson B, Wu K, Metcalfe J. 1984. An Inexpensive Remote Snow Depth Gauge: An Assessment. In: 52nd Annual Western Snow Conference, pp: 188-191.

Haan CT, Allred B, Storm DE, Sabbagh GJ, Prabhu S. 1995. Statistical Procedure for Evaluating Hydrologic Water-Quality Models. Transactions of the Asae, **38**: 725-733.

Hansen S, Davies MA. 2002. Windshields for Precipitation Gauges and Improved Measurement Technique for Snowfall. Agriculture USDo (ed.), pp: 1-6.

Harmel RD, Smith PK. 2007. Consideration of measurement uncertainty in the evaluation of goodness-of-fit in hydrologic and water quality modeling. Journal of Hydrology, **337**: 326-336.

Holman JP. 2001. Experimental Methods for Engineers. 7th Edn., McGraw-Hill.

Jonas T, Marty C, Magnusson J. 2009. Estimating the snow water equivalent from snow depth measurements in the Swiss Alps. Journal of Hydrology, **378**: 161-167.

Jost G, Weiler M, Gluns DR, Alila Y. 2007. The influence of forest and topography on snow accumulation and melt at the watershed-scale. Journal of Hydrology, **347**: 101-115.

Kunkel KE, Palecki MA, Hubbard KG, Robinson DA, Redmond KT, Easterling DR. 2007. Trend identification in twentieth-century US snowfall: The challenges. Journal of Atmospheric and Oceanic Technology, **24**: 64-73.

Larson LW, Peck EL. 1974. ACCURACY OF PRECIPITATION MEASUREMENTS FOR HYDROLOGIC MODELING. Water Resources Research, **10**: 857-863.

Martinec J, Rango A, Roberts R. 2008. Snowmelt Runoff Model (SRM) User's Manual.

Pagano T, Garen D. 2005. A recent increase in western US streamflow variability and persistence. Journal of Hydrometeorology, **6**: 173-179.

Peck EL. 1997. Quality of hydrometeorological, data in cold regions. Journal of the American Water Resources Association, **33**: 125-134.

Potter K, Kniss J, Riesenfeld R, Johnson CR. 2010. Visualizing Summary Statistics and Uncertainty. Computer Graphics Forum, **29**: 823-832.

Reichle RH, Walker JP, Koster RD, Houser PR. 2002. Extended versus ensemble Kalman filtering for land data assimilation. Journal of Hydrometeorology, **3**: 728-740.

Ryan WA, Doesken NJ, Fassnacht SR. 2008. Evaluation of ultrasonic snow depth sensors for U.S. snow measurements. Journal of Atmospheric and Oceanic Technology, **25**: 667-684.

Ryan WA, Doesken NJ, Fassnacht SR. 2008. Preliminary results of ultrasonic snow depth sensor testing for National Weather Service (NWS) snow measurements in the US. Hydrological Processes, **22**: 2748-2757.

Sevruk B, Ondras M, Chvila B. 2009. The WMO precipitation measurement intercomparisons. Atmospheric Research, **92**: 376-380.

Shallcross AT, McNamara JP, Flores AN, Marshall H, Marks DG, Glenn NF. 2010. Estimating Basin Snow Volume Using Aerial LiDAR and Binary Regression Trees. In: American Geophysical Union.

Slater AG, Clark MP. 2006. Snow data assimilation via an ensemble Kalman filter. Journal of Hydrometeorology, **7**: 478-493.

Sturm M, Taras B, Liston GE, Derksen C, Jonas T, Lea J. 2010. Estimating Snow Water Equivalent Using Snow Depth Data and Climate Classes. Journal of Hydrometeorology, **11**: 1380-1394.

Vicens GJ, Rodriguez-Iturbe I, Schaake JC. 1975. BAYESIAN FRAMEWORK FOR USE OF REGIONAL INFORMATION IN HYDROLOGY. Water Resources Research, **11**: 405-414.

Williams CJ, McNamara JP, Chandler DG. 2009. Controls on the temporal and spatial variability of soil moisture in a mountainous landscape: the signature of snow and complex terrain. Hydrology and Earth System Sciences, **13**: 1325-1336.

Yang DQ, Kane DL, Hinzman LD, Goodison BE, Metcalfe JR, Louie PYT, Leavesley GH, Emerson DG, Hanson CL. 2000. An evaluation of the Wyoming gauge system for snowfall measurement. Water Resources Research, **36**: 2665-2677.

APPENDIX A

Manufacturer Specifications for the XL-MaxSonar EZ2

LV-MaxSonar®-WR1™ High Performance Weather Resistant Sonar Range Finder

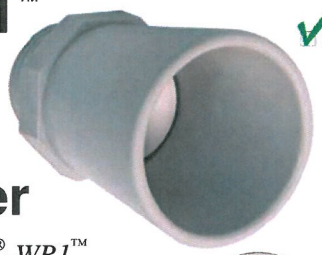

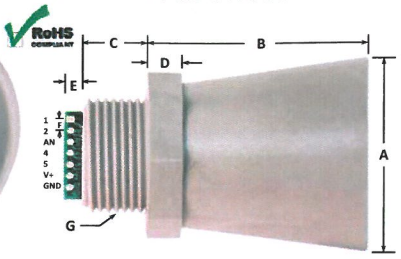

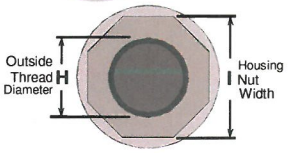

With 3V - 5.5V power the LV-MaxSonar®-WR1™ provides very short to long-range detection and ranging, in a compact, robust PVC housing, designed to meet IP67 water intrusion, and matches standard electrical ¾" PCV pipe fittings.

The LV-MaxSonar®-WR1™ detects objects from 0-inches to 254-inches (6.45-meters) and provides sonar range information from 12-inches out to 254-inches with 1-inch resolution. Objects from 0-inches to 12-inches range as 12-inches. The interface output formats included are pulse width output, analog voltage output, and serial digital output.

A	1.72" dia.	43.8 mm dia.
B	2.00"	50.7 mm
C	0.58"	14.4 mm
D	0.31"	7.9 mm
E	0.18"	4.6 mm
F	0.1"	2.54 mm
G	3/4" National Pipe Thread Straight	
H	1.032" dia.	26.2 mm dia.
I	1.37"	34.8 mm
weight, 1.76 oz., 50 grams		

values are nominal

Features

- Designed for outdoor or indoor environments
- Precise narrow beam
- High sensitivity
- Continuously variable gain
- Object detection includes zero range objects
- 3V to 5.5V supply with very low average current draw
- Readings can occur up to every 50mS, (20-Hz rate)
- Free run operation can continually measure and output range information
- Triggered operation provides the range reading as desired
- All interfaces are active simultaneously
  - Serial, 0 to Vcc
    - 9600Baud, 81N
  - Analog, (Vcc/512) / inch
  - Pulse width, (147uS/inch)
- Learns ringdown pattern when commanded to start ranging
- Sensor operates at 42KHz
- High output sine wave sensor drive

Benefits

- Very low cost IP67 sealed sonar ranger
- Reliable and stable range data
- Sensor dead zone virtually gone
- Lowest power IP67 ranger
- Quality narrow beam characteristics
- Easy hole mounting or mating with standard electrical fittings
- Very low power ranger, excellent for multiple sensor or battery based systems
- Can be triggered externally or internally
- Sensor reports the range reading directly, frees up user processor
- Fast measurement cycle
- User can choose any of the three sensor outputs

Beam Characteristics

People detection requires high sensitivity, yet minimal side-lobes requires low sensitivity. The LV-MaxSonar®-WR1™ balances the detection of people with minimal side-lobes.

Sample results for measured beam patterns are shown below on a 12-inch grid. The detection pattern is shown for;

(A) 0.25-inch diameter dowel,

(B) 1-inch diameter dowel, note the long narrow detection pattern,

(C) 3.25-inch diameter rod, note the long controlled detection pattern,

(D) 11-inch wide board moved left to right with the board parallel to the front sensor face and the sensor stationary. This shows the sensor's range capability.

Note: The displayed beam width of (D) is a function of the specular nature of sonar and the shape of the board (i.e. flat mirror like) and should never be confused with actual sensor beam width.

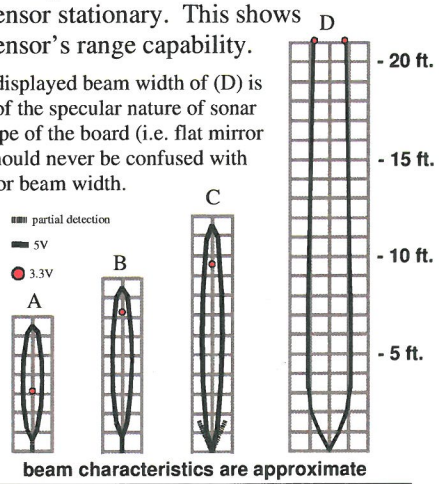

beam characteristics are approximate

MaxBotix® Inc.

4613 County Road 8, Brainerd, MN, 56401 USA
Email: info@maxbotix.com Web: www.maxbotix.com

LV-MaxSonar®-WR1™ Pin Out

Pin 1 - Leave open (or high) for serial output on the Pin 5 output. When pin one is held low the Pin 5 output sends a pulse (instead of serial data), suitable for low noise chaining.

Pin 2 - (PW) This pin outputs a pulse width representation of range. To calculate distance use the scale factor of 147uS per inch.

AN - Outputs analog voltage with a scaling factor of (Vcc/512) per inch. A supply of 5V yields ~9.8mV/in. and 3.3V yields ~6.4mV/in. The output is buffered and corresponds to the most recent range data.

Pin 4 - (RX) This pin is internally pulled high. The WR1™ will continually measure range and output if the pin is left unconnected or held high. If held low the WR1™ will stop ranging. Bring high 20uS or more for range reading.

Pin 5 - (TX) When Pin 1 is open or held high, the Pin 5 output delivers asynchronous serial with an RS232 format, except voltages are 0-Vcc. The output is an ASCII capital "R", followed by three ASCII character digits representing the range in inches up to a maximum of 255, followed by a carriage return (ASCII 13). The baud rate is 9600, 8 bits, no parity, with one stop bit. Although the voltage of 0-Vcc is outside the RS232 standard, most RS232 devices have sufficient margin to read 0-Vcc serial data. If standard voltage level RS232 is desired, invert, and connect an RS232 converter such as a MAX232.
When Pin 1 is held high the TX output sends a single pulse, suitable for low noise chaining (no serial data).

V+ Operates on 3V - 5.5V. Average (and peak) current draw for 3.3V & 5V operation is 2.1mA (50mA peak) & 3.4mA (100mA peak) respectively. Peak current is used during sonar pulse transmit.

GND Return for the DC power supply. GND (& V+) must be ripple and noise free for best operation.

LV-MaxSonar®-WR1™ Circuit

The LV-MaxSonar®-WR1™ sensor functions using active components consisting of an LM324 and PIC16F690, together with a variety of other components. The schematic is shown to provide the user with detailed connection information.

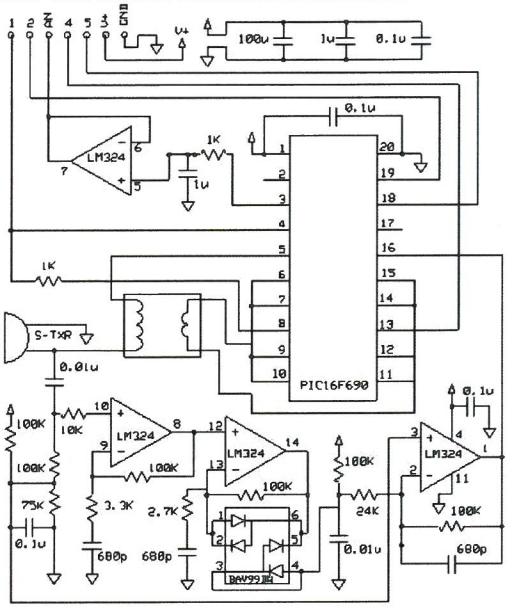

LV-MaxSonar®-WR1™ Timing Description

320mS after power-up, the LV-MaxSonar®-WR1™ is ready to accept the command to range. If Pin 4 is left open or held high, the sensor will first run a calibration cycle (49mS), and then it will take a range reading (49mS). Therefore, the first reading will take ~100mS. Subsequent readings will take 49mS. The LV-MaxSonar®-WR1™ checks Pin 4 at the end of every cycle. Range data can be acquired once every 49mS.

Each ranging cycle of a 49mS period starts by Pin 4 being high or open, after which the LV-MaxSonar®-WR1™ sends thirteen 42KHz waves, after which the pulse width Pin 2 is set high. When a target is detected, Pin 2 is pulled low. Pin 2 pin is high for up to 37.5mS if no target is detected. The remainder of the 49mS time (less 4.7mS) is spent adjusting the analog voltage to the correct level. When a long distance is measured immediately after a short distance reading, the analog voltage may not reach the exact level within one read cycle. During the last 4.7mS, the serial data is sent. The LV-MaxSonar®-WR1™ timing is factory calibrated, and in use is better than two percent.

LV-MaxSonar®-WR1™ General Power-Up Instruction

Each time after the LV-MaxSonar®-WR1™ is powered up, it will calibrate during its first read cycle. The sensor uses this stored information to range a close object. It is important that objects not be close to the sensor during this calibration cycle. The best sensitivity is obtained when it is clear for eighteen inches, but good results are common when clear for at least twelve inches. If an object is too close during the calibration cycle, the sensor may then ignore objects at that distance.

The LV-MaxSonar®-WR1™ does not use the calibration data to temperature compensate for range, but instead to compensate for the sensor ringdown pattern. If the temperature, humidity, or applied voltage changes during operation, the sensor may require recalibration to reacquire the ringdown pattern. Unless recalibrated, if the temperature increases, the sensor is more likely to have false close readings. If the temperature decreases, the sensor is more likely to have reduced up close sensitivity. To recalibrate the LV-MaxSonar®-WR1™, cycle power, then command a read cycle.

MaxBotix® Inc.
4613 County Road 8, Brainerd, MN, 56401 USA
Email: info@maxbotix.com Web:www.maxbotix.com

APPENDIX B

Manufacturer Specifications for the GE-MCS Thermistor

NTC THERMISTORS: TYPE C100

EPOXY COATED CHIP THERMISTOR

DESCRIPTION:

Epoxy Coated chip thermistors with bare tinned copper lead-wires.

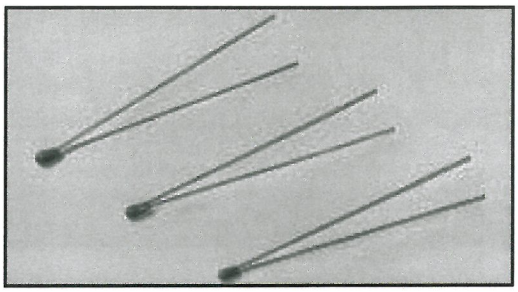

FEATURES:

- Low cost, solid state temperature sensor
- Point matched at 25°C to ±1%, ±2%, ±5% or ±10%
- Suitable for use over range of –80°C to +150°C
- High sensitivity greater than –4%/°C at 25°C
- Suitable for temperature measurement, control and compensation
- High reliability and stability
- Resin coated for good mechanical strength and resistance to solvents
- .012" (.3 mm) dia. bare tinned copper lead-wires

DIMENSIONS:

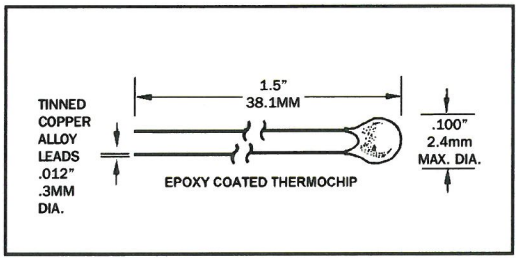

Select appropriate part number below for resistance and temperature tolerance desired

$R_{25°C}$	MATERIAL SYSTEM	$R_{25°C}$ ± 1%	$R_{25°C}$ ± 2%	$R_{25°C}$ ± 5%	$R_{25°C}$ ± 10%
2000	F	C100F202F	C100F202G	C100F202J	C100F202K
2252	F	C100F232F	C100F232G	C100F232J	C100F232K
3000	F	C100F302F	C100F302G	C100F302J	C100F302K
5000	F	C100F502F	C100F502G	C100F502J	C100F502K
10000	F	C100F103F	C100F103G	C100F103J	C100F103K
10000	Y	C100Y103F	C100Y103G	C100Y103J	C100Y103K
15000	F	C100F153F	C100F153G	C100F153J	C100F153K
20000	F	C100F203F	C100F203G	C100F203J	C100F203K
30000	H	C100H303F	C100H303G	C100H303J	C100H303K
50000	G	C100G503F	C100G503G	C100G503J	C100G503K
100000	Y	C100Y104F	C100Y104G	C100Y104J	C100Y104K
100000	G	C100G104F	C100G104G	C100G104J	C100G104K

OPTIONS:

Consult factory for availability of options:

- Other resistance values in the range of 100Ω - 100kΩ
- Other tolerances
- Alternative lead lengths
- Other reference temperatures
- Alternative lead wires or lengths

DATA:

THERMAL AND ELECTRICAL PROPERTIES:

Dissipation constant:.....(still air) 1 mW/°C
(stirred oil) 8 mW/°C

Thermal time constant:.....(still air) 10 sec.
(stirred oil) 1 sec.

Maximum power at 25°C 75mW
(derated from 100% at 25°C to 0% at 100°C)

Crown Industrial Estate, Priorswood Road
Taunton, Somerset TA2 8QY UK
Tel +44 (0) 1823 335200
Fax +44 (0) 1823 332637

808 US Highway 1
Edison, New Jersey 08817-4695 USA
Tel +1 (732) 287 2870
Fax +1 (732) 287 8847

967 Windfall Road
St. Marys, Pennsylvania 15857-3397 USA
Tel +1 (814) 834 9140
Fax +1 (814) 781 7969

MATERIAL TYPE: F

AVAILABLE PRODUCTS:

HM, C100, EC95, DC95, MC65, MF65, SC30, SC50

Data for material type : F

Temp Range (°C)	Ratio	Beta
0 to 50	9.08	3895
0 to 70	18.64	3917
25 to 50	2.78	3933
25 to 85	9.30	3969
25 to 100	14.64	3981
25 to 125	29.05	3999
37.8 to 104.4	9.67	4000

To calculate Rt/R25 at temperatures other than those listed in the table, use the following equation:

$Rt/R25 = \exp\{A + B/T + C/T^2 + D/T^3\}$

where T = temperature in K

where K = °C + 273.15

Temp Range (°C)	A	B	C	D
-50 to 0	-1.4122478E+01	4.4136033E+03	-2.9034189E+04	-9.3875035E+06
0 to 50	-1.4141963E+01	4.4307830E+03	-3.4078983E+04	-8.8941929E+06
50 to 100	-1.4202172E+01	4.4975256E+03	-5.8421357E+04	-5.9658796E+06
100 to 150	-1.6154078E+01	6.8483992E+03	-1.0004049E+06	1.1961431E+08

To calculate the actual thermistor temperature as a function of the thermistor resistance, use the following equation:

$1/T = a + b(\text{Ln } Rt/R25) + c(\text{Ln } Rt/R25)^2 + d(\text{Ln } Rt/R25)^3$

Rt/R25 range	a	b	c	d
68.600 to 3.274	3.3538646E-03	2.5654090E-04	1.9243889E-06	1.0969244E-07
3.274 to 0.36036	3.3540154E-03	2.5627725E-04	2.0829210E-06	7.3003206E-08
0.36036 to 0.06831	3.3539264E-03	2.5609446E-04	1.9621987E-06	4.6045930E-08
0.06831 to 0.01872	3.3368620E-03	2.4057263E-04	-2.6687093E-06	-4.0719355E-07

†The deviation resulting from the tolerance on the material constant, Beta. The deviation must be added to the resistance tolerance of the part as specified at 25°C.

Temperature (°C)	Rt/R25 nominal	Temp Coef α (%/°C)	β Deviation† (±%)
-50	68.60	7.21%	2.30%
-45	48.16	6.96%	2.68%
-40	34.23	6.71%	2.87%
-35	24.62	6.48%	2.92%
-30	17.91	6.26%	2.86%
-25	13.17	6.05%	2.71%
-20	9.782	5.85%	2.50%
-15	7.339	5.66%	2.25%
-10	5.558	5.47%	1.97%
-5	4.247	5.30%	1.68%
0	3.274	5.13%	1.37%
5	2.544	4.97%	1.07%
10	1.992	4.81%	0.78%
15	1.572	4.67%	0.50%
20	1.250	4.53%	0.24%
25	1.000	4.39%	0.00%
30	0.8056	4.26%	0.21%
35	0.6530	4.14%	0.40%
40	0.5326	4.02%	0.56%
45	0.4369	3.91%	0.69%
50	0.3604	3.80%	0.80%
55	0.2989	3.69%	0.87%
60	0.2491	3.59%	0.92%
65	0.2087	3.49%	0.93%
70	0.1756	3.40%	0.92%
75	0.1485	3.31%	0.88%
80	0.1261	3.23%	0.81%
85	0.1075	3.14%	0.72%
90	0.09209	3.06%	0.59%
95	0.07916	2.99%	0.45%
100	0.06831	2.91%	0.28%
105	0.05916	2.85%	0.08%
110	0.05141	2.77%	0.12%
115	0.04483	2.70%	0.36%
120	0.03922	2.64%	0.61%
125	0.03442	2.57%	0.87%
130	0.03030	2.51%	1.16%
135	0.02675	2.47%	1.46%
140	0.02369	2.41%	1.82%
145	0.02103	2.35%	2.14%
150	0.01872	2.35%	2.46%

Crown Industrial Estate, Priorswood Road
Taunton, Somerset TA2 8QY UK
Tel +44 (0) 1823 335200
Fax +44 (0) 1823 332637

808 US Highway 1
Edison, New Jersey 08817-4695 USA
Tel +1 (732) 287 2870
Fax +1 (732) 287 8847

967 Windfall Road
St. Marys, Pennsylvania 15857-3397 USA
Tel +1 (814) 834 9140
Fax +1 (814) 781 7969

APPENDIX C

Example of Campbell Scientific Edlog Data Acquisition Program Used for the Treeline USD Sensor Network

TLPITSNOW_093011_Boe.csi, Table 1

```
43:  Do (P86)
 1: 10      Set Output Flag High (Flag 0)

44:  Set Active Storage Area (P80)
 1: 1       Final Storage Area 1
 2: 1       Array ID

45:  Real Time (P77)
 1: 1110    Year,Day,Hour/Minute (midnight = 0000)

46:  Sample (P70)
 1: 19      Reps
 2: 1       Loc [ ntdr10    ]

47:  Sample (P70)
 1: 14      Reps
 2: 30      Loc [ TDR1      ]

48:  Sample (P70)
 1: 1       Reps
 2: 44      Loc [ BATTERY   ]


49:  Serial Out (P96)
 1: 71      Storage Module


50:  Do (P86)
 1: 20      Set Output Flag Low (Flag 0)

51:  End (P95)

52:  If time is (P92)
 1: 0000    Minutes (Seconds --) into a
 2: 15      Interval (same units as above)
 3: 30      Then Do


;This loop performs single ended measurments on 6 thermistors followed by 20 snow depth measurements (5 active)
; AM16/32 set to "4x16". Three thermistors are attached to each set.
;One thermistor end is connected to Hodd, Lodd, and Heven in
;each set. The other ends are bundled in Leven.
;Depth sensor yellow wires (Vout) are connected to Heven, Hodd, and Lodd channels. Leven channels are left open.
;Multiplexor COM Hodd, Lodd, Hven, and Leven are connected toDatalogger SE1, SE2, SE3, and AG respectively.
;C5 is connected to reset, C6 to clock


;Reset the multiplexor (all channels open)

53:  Do (P86)
 1: 45      Set Port 5 High

;Begin the multiplexor loop for thermistors. The loop count is 2 because we are using 2 sets (2x3 = 6)
```

TLPITSNOW_093011_Boe.csi, Table 1

```
54:  Beginning of Loop (P87)
 1: 0000     Delay
 2: 2        Loop Count

;Clock the multiplor. This connects the next set to the datalogger.

55:  Do (P86)
 1: 76       Pulse Port 6

;Here add a step loop index. After each pass, the input location is incremented 3 times
;beyond the input location at the beginning of the last pass.

56:  Step Loop Index (P90)
 1: 3        Step

;Add a brief delay to allow the contacts to settle (ex2 is not actually used)
57:  Excitation with Delay (P22)
 1: 2        Ex Channel
 2: 1        Delay W/Ex (units = 0.01 sec)
 3: 1        Delay After Ex (units = 0.01 sec)
 4: 0        mV Excitation

;Perform the single ended measurement with excitation. 3 reps are used to measure SE1, SE2, and SE3.
;Now we have an index after the input location. Each location is indexed to increment internal storage.
;P4 with a .0005 multiplier stores the output voltage across the thermistor

58:  Excite-Delay (SE) (P4)
 1: 3        Reps
 2: 25       2500 mV 60 Hz Rejection Range (Delay must be zero)
 3: 1        SE Channel
 4: 1        Excite all reps w/Exchan 1
 5: 1        Delay (units 0.01 sec)
 6: 2000     mV Excitation
 7: 51    -- Loc [ Rt1      ]
 8: .0005    Mult
 9: 0.0      Offset


59:  Z=X (P31)
 1: 51    -- X Loc [ Rt1      ]
 2: 45    -- Z Loc [ Tvolt1_1  ]


;Bridge transform converts voltage to resistance using 10K resistors

60:  BR Transform Rf[X/(1-X)] (P59)
 1: 3        Reps
 2: 51    -- Loc [ Rt1      ]
 3: 10000    Multiplier (Rf)

61:  End (P95)

;Convert resistance to temperature
```

TLPITSNOW_093011_Boe.csi, Table 1

```
;store constants for conversion from resistance to temperature


62:  Z=F x 10^n (P30)
 1: -1.41225 F
 2: 1        n, Exponent of 10
 3: 116      Z Loc [ a        ]

63:  Z=F x 10^n (P30)
 1: 4.4136   F
 2: 3        n, Exponent of 10
 3: 117      Z Loc [ b        ]


;calculate Rt/R25

64:  Beginning of Loop (P87)
 1: 0000     Delay
 2: 6        Loop Count

;R25 = 10,000

    65:  Z=X*F (P37)
     1: 51    -- X Loc [ Rt1      ]
     2: .0001    F
     3: 63    -- Z Loc [ temp1    ]

;ln of rt/r25


    66:  Z=LN(X) (P40)
     1: 63    -- X Loc [ temp1    ]
     2: 63    -- Z Loc [ temp1    ]

;denominator in T equation


    67:  Z=X-Y (P35)
     1: 63    -- X Loc [ temp1    ]
     2: 116      Y Loc [ a        ]
     3: 63    -- Z Loc [ temp1    ]

;Calculate T

    68:  Z=X/Y (P38)
     1: 117      X Loc [ b        ]
     2: 63    -- Y Loc [ temp1    ]
     3: 63    -- Z Loc [ temp1    ]

69:  End (P95)


;Begin loop for Maxbotix sensors
```

TLPITSNOW_093011_Boe.csi, Table 1

```
70:  Beginning of Loop (P87)
 1: 0000     Delay
 2: 02       Loop Count

;clock the multiplexor

    71:  Do (P86)
     1: 76       Pulse Port 6


;Here add a step loop index. After each pass, the input location is incremented x times
;beyond the input location at the beginning of the last pass.


72:  Step Loop Index (P90)
 1: 3        Step

;measure Maxbotix loop
73:  Volt (SE) (P1)
 1: 3        Reps
 2: 25       2500 mV 60 Hz Rejection Range
 3: 1        SE Channel
 4: 69     -- Loc [ rawdpth1  ]
 5: .20408   Multiplier
 6: 0.0      Offset


74:  End (P95)


;determining distance between sensor and snow in terms of voltage
75:  Z=X*F (P37)
 1: 69       X Loc [ rawdpth1  ]
 2: 4.90004  F
 3: 57       Z Loc [ Dvolt1    ]

76:  Z=X*F (P37)
 1: 70       X Loc [ rawdpth2  ]
 2: 4.90004  F
 3: 58       Z Loc [ Dvolt2    ]

77:  Z=X*F (P37)
 1: 71       X Loc [ rawdpth3  ]
 2: 0.0      F
 3: 59       Z Loc [ Dvolt3    ]

78:  Z=X*F (P37)
 1: 72       X Loc [ rawdpth4  ]
 2: 0.0      F
 3: 60       Z Loc [ Dvolt4    ]
```

TLPITSNOW_093011_Boe.csi, Table 1

79: Z=X*F (P37)
1: 73 X Loc [rawdpth5]
2: 0.0 F
3: 61 Z Loc [Dvolt5]

;compensate for temperature (later)

80: Do (P86)
1: 55 Set Port 5 Low

81: Do (P86)
1: 10 Set Output Flag High (Flag 0)

82: Set Active Storage Area (P80)
1: 1 Final Storage Area 1
2: 2 Array ID

83: Real Time (P77)
1: 1110 Year,Day,Hour/Minute (midnight = 0000)

84: Sample (P70)
1: 5 Reps
2: 45 Loc [Tvolt1_1]

85: Sample (P70)
1: 5 Reps
2: 57 Loc [Dvolt1]

86: Sample (P70)
1: 5 Reps
2: 69 Loc [rawdpth1]

87: Serial Out (P96)
1: 71 Storage Module

88: Do (P86)
1: 20 Set Output Flag Low (Flag 0)

89: End (P95)

*Table 2 Program

TLPITSNOW_093011_Boe.csi, Table 2

01: 60 Execution Interval (seconds)

*Table 3 Subroutines

End Program

TLPITSNOW_093011_Boe.csi, Input Locations

Addr	Name	Flags	# Reads	# Writes	Blocks
1	[ntdr10]	RWM-	1	1	Start ------ ---
2	[ntdr20]	R-M-	1	0	----- ------ ---
3	[ntdr30]	RWM-	1	1	----- Member ---
4	[ntdr40]	RWM-	1	1	----- Member ---
5	[ntdr50]	RWM-	1	1	----- Member ---
6	[ntdr71]	RWM-	1	1	----- Member ---
7	[ntdr72]	RWM-	1	1	----- Member ---
8	[ntdr75]	RWM-	1	1	----- Member ---
9	[ntdr76]	RWM-	1	1	----- Member ---
10	[ntdr77]	RWM-	1	1	----- Member ---
11	[ntdr11]	RWM-	1	1	----- Member ---
12	[ntdr78]	RWM-	1	1	----- Member ---
13	[ntdr81]	RWM-	1	1	----- Member ---
14	[ntdr82]	RWM-	1	1	----- Member ---
15	[ntdr83]	RWM-	1	1	----- Member ---
16	[ntdr84]	RWM-	1	1	----- Member ---
17	[ntdr85]	RWM-	1	1	----- Member ---
18	[ntdr86]	RWM-	1	1	----- Member ---
19	[ntdr87]	RWM-	1	1	----- ------ End
20	[_____]	----	0	0	----- ------ ---
21	[TC_1]	--M-	0	0	----- ------ ---
22	[TC_2]	--M-	0	0	----- ------ ---
23	[TC_3]	--M-	0	0	----- ------ ---
24	[TC_4]	--M-	0	0	----- ------ ---
25	[FLUX_1]	--M-	0	0	----- ------ ---
26	[FLUX_2]	--M-	0	0	----- ------ End
27	[REFTEMP]	----	0	0	----- ------ ---
28	[_____]	----	0	0	----- ------ ---
29	[_____]	----	0	0	----- ------ ---
30	[TDR1]	RWM-	1	1	Start ------ ---
31	[TDR2]	RWM-	1	1	----- Member ---
32	[TDR3]	RWM-	1	1	----- Member ---
33	[TDR4]	RWM-	1	1	----- ------ End
34	[TDR71]	RW--	1	1	----- ------ ---
35	[TDR72]	RW--	1	1	----- ------ ---
36	[TDR73]	RW--	1	1	----- ------ ---
37	[TDR74]	RW--	1	1	----- ------ ---
38	[TDR75]	RW--	1	1	----- ------ ---
39	[TDR76]	RW--	1	1	----- ------ ---
40	[TDR77]	RW--	1	1	----- ------ ---
41	[TDR78]	RW--	1	1	----- ------ ---
42	[TDR81]	RW--	1	1	----- ------ ---
43	[TDR82]	RW--	1	1	----- ------ ---
44	[BATTERY]	RW--	1	1	----- ------ ---
45	[Tvolt1_1]	RW--	1	1	----- ------ ---
46	[Tvolt1_2]	R---	1	0	----- ------ ---
47	[Tvolt1_3]	R---	1	0	----- ------ ---
48	[_____]	R---	1	0	----- ------ ---
49	[_____]	R---	1	0	----- ------ ---
50	[_____]	----	0	0	----- ------ ---
51	[Rt1]	RW--	3	2	Start ------ ---
52	[rt2]	RW--	1	2	----- Member ---

TLPITSNOW_093011_Boe.csi, Input Locations

53	[rt3]	RW--	1	2	-----	------	End
54	[rt4]	----	0	0	-----	------	---
55	[rt5]	----	0	0	-----	------	---
56	[rt6]	----	0	0	-----	------	---
57	[Dvolt1]	RW--	1	1	-----	------	---
58	[Dvolt2]	RW--	1	1	-----	------	---
59	[Dvolt3]	RW--	1	1	-----	------	---
60	[Dvolt4]	RW--	1	1	-----	------	---
61	[Dvolt5]	RW--	1	1	-----	------	---
62	[_____]	----	0	0	-----	------	---
63	[temp1]	RW--	3	4	-----	------	---
64	[temp2]	----	0	0	-----	------	---
65	[temp3]	----	0	0	-----	------	---
66	[temp4]	----	0	0	-----	------	---
67	[temp5]	----	0	0	-----	------	---
68	[temp6]	----	0	0	-----	------	---
69	[rawdpth1]	RW--	3	1	Start	------	---
70	[rawdpth2]	RW--	2	1	-----	Member	---
71	[rawdpth3]	RW--	2	1	-----	------	End
72	[rawdpth4]	R---	2	0	-----	------	---
73	[rawdpth5]	R---	2	0	-----	------	---
74	[rawdpth6]	----	0	0	-----	------	---
75	[_____]	----	0	0	-----	------	---
76	[_____]	----	0	0	-----	------	---
77	[_____]	----	0	0	-----	------	---
78	[_____]	----	0	0	-----	------	---
79	[_____]	----	0	0	-----	------	---
80	[_____]	----	0	0	-----	------	---
81	[_____]	----	0	0	-----	------	---
82	[_____]	----	0	0	-----	------	---
83	[_____]	----	0	0	-----	------	---
84	[_____]	----	0	0	-----	------	---
85	[_____]	----	0	0	-----	------	---
86	[_____]	----	0	0	-----	------	---
87	[_____]	----	0	0	-----	------	---
88	[_____]	----	0	0	-----	------	---
89	[_____]	----	0	0	-----	------	---
90	[_____]	----	0	0	-----	------	---
91	[_____]	----	0	0	-----	------	---
92	[_____]	----	0	0	-----	------	---
93	[_____]	----	0	0	-----	------	---
94	[_____]	----	0	0	-----	------	---
95	[_____]	----	0	0	-----	------	---
96	[_____]	----	0	0	-----	------	---
97	[_____]	----	0	0	-----	------	---
98	[_____]	----	0	0	-----	------	---
99	[_____]	----	0	0	-----	------	---
100	[_____]	----	0	0	-----	------	---
101	[_____]	R---	1	0	-----	------	---
102	[_____]	R---	1	0	-----	------	---
103	[_____]	R---	1	0	-----	------	---
104	[_____]	R---	1	0	-----	------	---
105	[_____]	R---	1	0	-----	------	---
106	[_____]	R---	1	0	-----	------	---

TLPITSNOW_093011_Boe.csi, Input Locations

```
107   [ __________ ] R---  1     0     ----- ------ ---
108   [ __________ ] R---  1     0     ----- ------ ---
109   [ __________ ] R---  1     0     ----- ------ ---
110   [ __________ ] R---  1     0     ----- ------ ---
111   [ __________ ] R---  1     0     ----- ------ ---
112   [ __________ ] R---  1     0     ----- ------ ---
113   [ __________ ] R---  1     0     ----- ------ ---
114   [ __________ ] R---  1     0     ----- ------ ---
115   [ ntdr1    ] ----  0     0     ----- ------ ---
116   [ a        ] RW--  1     1     ----- ------ ---
117   [ b        ] RW--  1     1     ----- ------ ---
118   [ b2       ] ----  0     0     ----- ------ ---
119   [ b3       ] ----  0     0     ----- ------ ---
```